# ORIGINAL RESEARCH

Mouse Model of Mutated in Colorectal Cancer Gene Deletion Reveals Novel Pathways in Inflammation and Cancer

Nicola Currey,[1,*] Zeenat Jahan,[1,*] C. Elizabeth Caldon,[1,2] Phuong N. Tran,[1,2] Fahad Benthani,[1,2] Penelope De Lacavalerie,[1,2] Daniel L. Roden,[1,2] Brian S. Gloss,[1,2] Claudia Campos,[3] Elaine G. Bean,[4] Amanda Bullman,[4] Saskia Reibe-Pal,[1] Marcel E. Dinger,[1,2] Mark A. Febbraio,[1,2] Stephen J. Clarke,[5] Jane E. Dahlstrom,[4] and Maija R. J. Kohonen-Corish[1,6,7]

[1]Garvan Institute of Medical Research, Sydney, New South Wales, Australia; [2]St Vincent's Clinical School, [7]Microbiome Research Centre, St George and Sutherland Clinical School, University of New South Wales, Sydney, New South Wales, Australia; [3]Instituto Gulbenkian de Ciência, Oeiras, Portugal; [4]ACT Pathology, The Canberra Hospital, Australian National University Medical School, Canberra, Australian Capital Territory, Australia; [5]Royal North Shore Hospital, University of Sydney, Sydney, New South Wales, Australia; [6]School of Medicine, Western Sydney University, Sydney, New South Wales, Australia
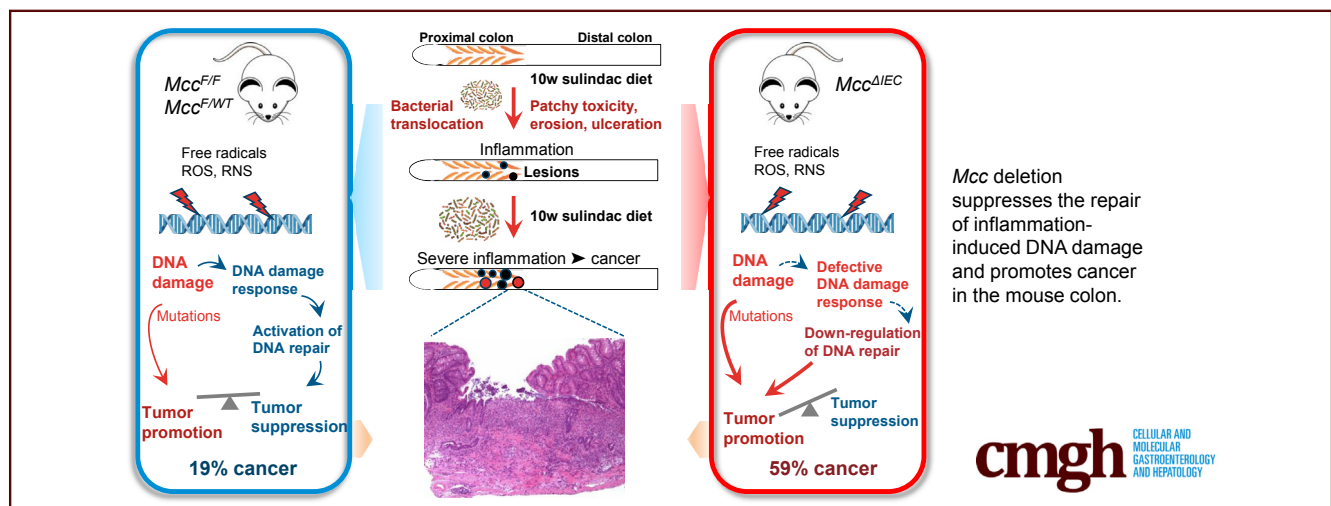
SUMMARY

A new *Mcc*-knockout mouse model shows impairment of DNA repair pathways in drug-induced inflammatory lesions leading to cancer development. The lesions show a strong interferon-γ response regardless of *Mcc* expression, including novel *Irg* genes not previously described in the mouse colon.

BACKGROUND & AIMS: The early events by which inflammation promotes cancer are still not fully defined. The *MCC* gene is silenced by promoter methylation in colitis-associated and sporadic colon tumors, but its functional significance in precancerous lesions or polyps is not known. Here, we aimed to determine the impact of *Mcc* deletion on the cellular pathways and carcinogenesis associated with inflammation in the mouse proximal colon.

METHODS: We generated knockout mice with deletion of *Mcc* in the colonic/intestinal epithelial cells ($Mcc^{\Delta IEC}$) or in the whole body ($Mcc^{\Delta/\Delta}$). Drug-induced lesions were analyzed by transcriptome profiling (at 10 weeks) and histopathology (at 20 weeks). Cell-cycle phases and DNA damage proteins were analyzed by flow cytometry and Western blot of hydrogen peroxide–treated mouse embryo fibroblasts.

RESULTS: Transcriptome profiling of the lesions showed a strong response to colon barrier destruction, such as up-regulation of key inflammation and cancer-associated genes as well as 28 interferon γ–induced guanosine triphosphatase genes, including the homologs of Crohn's disease susceptibility gene *IRGM*. These features were shared by both *Mcc*-expressing and *Mcc*-deficient mice and many of the altered gene expression pathways were similar to the mesenchymal colorectal cancer subtype known as consensus molecular subtype 4 (CMS4). However, *Mcc* deletion was required for increased carcinogenesis in the lesions, with adenocarcinoma in 59% of $Mcc^{\Delta IEC}$ compared with 19% of *Mcc*-expressing mice ($P = .002$). This was not accompanied by hyperactivation of β-catenin, but *Mcc* deletion caused down-regulation of DNA repair genes and a disruption of DNA damage signaling.

CONCLUSIONS: Loss of *Mcc* may promote cancer through a failure to repair inflammation-induced DNA damage. We provide a comprehensive transcriptome data set of early colorectal lesions and evidence for the in vivo significance of *MCC* silencing in colorectal cancer. *(Cell Mol Gastroenterol Hepatol 2019;7:819–839; https://doi.org/10.1016/j.jcmgh.2019.01.009)*

Keywords: E2F Targets; DNA Repair; IFNγ-Induced GTPases; CMS4.

The role of inflammation as a risk factor and promoter of colorectal cancer is under intense investigation, both in colitis-associated cancer (CAC) and in sporadic tumors. There are several mouse models that have shown valuable novel insights into the etiology of CAC, but the molecular mechanisms and early events by which inflammation promotes cancer still are poorly understood.[1]

The *MCC* gene was discovered as a result of its proximity to *APC* on chromosome 5,[2] but its possible significance in carcinogenesis was overlooked until recently.[3–9] In colorectal cancers, a common alteration is promoter methylation that causes *MCC* silencing,[3,4,10] most frequently in cancers of the proximal colon (58%).[11] The *MCC* defect appears early in premalignant tumors or lesions and is strongly associated with sessile serrated polyps (80%–86%).[4,12,13] *Mcc* mutations were identified as drivers of colon or liver carcinogenesis in transposon-based genetic screens in mice,[14,15] but it has not been reported whether mutated in colorectal cancer (MCC) deficiency predisposes to cancer in premalignant colon tumors or lesions.

To further determine the role of MCC in carcinogenesis in vivo, we generated new knockout mouse models for *Mcc*. We focused on the mouse colon and hypothesized that loss of MCC would have an impact on inflammation-associated carcinogenesis in the proximal colon. Therefore, we exploited the drug sulindac, which acts as an irritant in a short region of the mouse proximal colon.[16–18] This highly localized side effect of sulindac is independent of its chemopreventive activity in experimental models of colon cancer.[16,19–21] Initially, exposure to sulindac causes microscopic foci of surface tissue erosion. With long-term administration of the drug (10–20 wk), the foci develop into visible ulcerated lesions with chronic inflammation that are surrounded by normal tissue. Most of these lesions are benign but can develop into adenocarcinoma in strains of knockout mice with tumor-suppressor gene defects, such as *Apc*, *p53*, *Msh2*, and *Mlh1*.[16,19,21,22] Here, we show that *Mcc* deficiency promotes carcinogenesis in this model through failure to repair inflammation-induced DNA damage.

Results

Generation of Mcc^F/F, Mcc^ΔIEC, and Mcc^Δ/Δ Mice

A new *Mcc*-loxP (*Mcc*^F/F) mouse line was developed using a gene-targeting approach (Figure 1A) and designated B6.Cg-Mcc<tm1Maija>/Ausb (*Mcc*^F/F). We generated both whole-body knockout (*Mcc*^Δ/Δ) and conditional knockout mice *Vilcre-Mcc*^F/F, with loss of *Mcc* expression in the colonic

and intestinal epithelial cells (*Mcc*^ΔIEC). The *Villin-cre* transgene expresses cre constitutively in the epithelial cells of the entire crypt-villus axis along the small and large intestine, but we focused on the effect of *Mcc* deletion in the colon.[23] *Mcc* expression was reduced significantly in the mucosal layer throughout the colon in the homozygous *Mcc*^ΔIEC mice (Figure 1B). Histopathology of major organs showed no gross abnormalities or tumors in the whole-body knockout *Mcc*^Δ/Δ mice, and there was no reduced survival after a 12-month follow-up period. However, histopathology analysis of bromodeoxyuridine (BrdU) incorporation in vivo showed that there was a 10%–20% decrease in the proliferation rate of colon epithelial cells in *Mcc*^Δ/Δ mice compared with their wild-type (WT) siblings (Figure 1C).

Mcc *Deficiency Drives Inflammation-Associated Cancer*

Mcc^ΔIEC, *Mcc*^ΔIEC/WT, and their genotype controls (*Mcc*^F/F and *Mcc*^F/WT) were given feed containing sulindac or control feed for 20 weeks. As expected, sulindac exposure caused the development of macroscopic lesions in the mucosal folds of the proximal colon. Both *Mcc*-expressing and *Mcc*-deficient mice developed these drug-induced lesions and there was no difference in the size or number of the lesions, or the area of the colon affected, indicating a similar level of macroscopic tissue damage (Figure 1D). The lesions were mostly found in a 1-cm region of the proximal colon that previously was designated as P2 and is located 2–3 cm from the cecum.[16] Microscopically, the lesions featured mucosal surface erosion or ulceration with mixed inflammatory cell infiltrate, resulting in mild-moderate to severe acute or chronic inflammation, similar to our previous reports on this model.[16,18] A subset of up to 4 lesions/mouse developed mucinous or nonmucinous adenocarcinoma. The frequency of cancer was 59% (13 of 22) in the homozygous *Mcc*^ΔIEC mice, 35% (7 of 20) in the heterozygous knockout *Mcc*^ΔIEC/WT, and 19% (8 of 42) in the *Mcc*-expressing genotype controls (combined *Mcc*^F/F and *Mcc*^F/WT). Loss of *Mcc* expression increased carcinogenesis (*P* = .002; *Mcc*^ΔIEC vs *Mcc*-expressing controls). This was owing to an

increase of cancer in $Mcc^{\Delta IEC}$ males (10 of 12) compared with Mcc-expressing males (5 of 16; $P = .009$). Overall, cancer was more common in sulindac-treated males (21 of 41) than in females (7 of 43) ($P = .001$). This was statistically significant in the 13 $Mcc^{\Delta IEC}$ mice with cancer (10 of 12 males vs 3 of 10 females; $P = .03$), but not in the Mcc-expressing group with only 8 cancers (5 of 16 males vs 3 of 26 females; $P = .22$). Representative adenocarcinoma is shown in Figure 1E.

Drug-Induced Colon Lesions Show Up-Regulation of Proinflammatory Genes and Down-Regulation of β-Catenin Target Genes

To determine gene expression changes in the earlier lesions we conducted transcriptome profiling after 10 weeks of sulindac exposure. The surface mucosa was harvested from proximal (P1, P2) and distal colon and micro-dissected separately from the macroscopic lesions. Hundreds of genes were up-regulated in the lesions
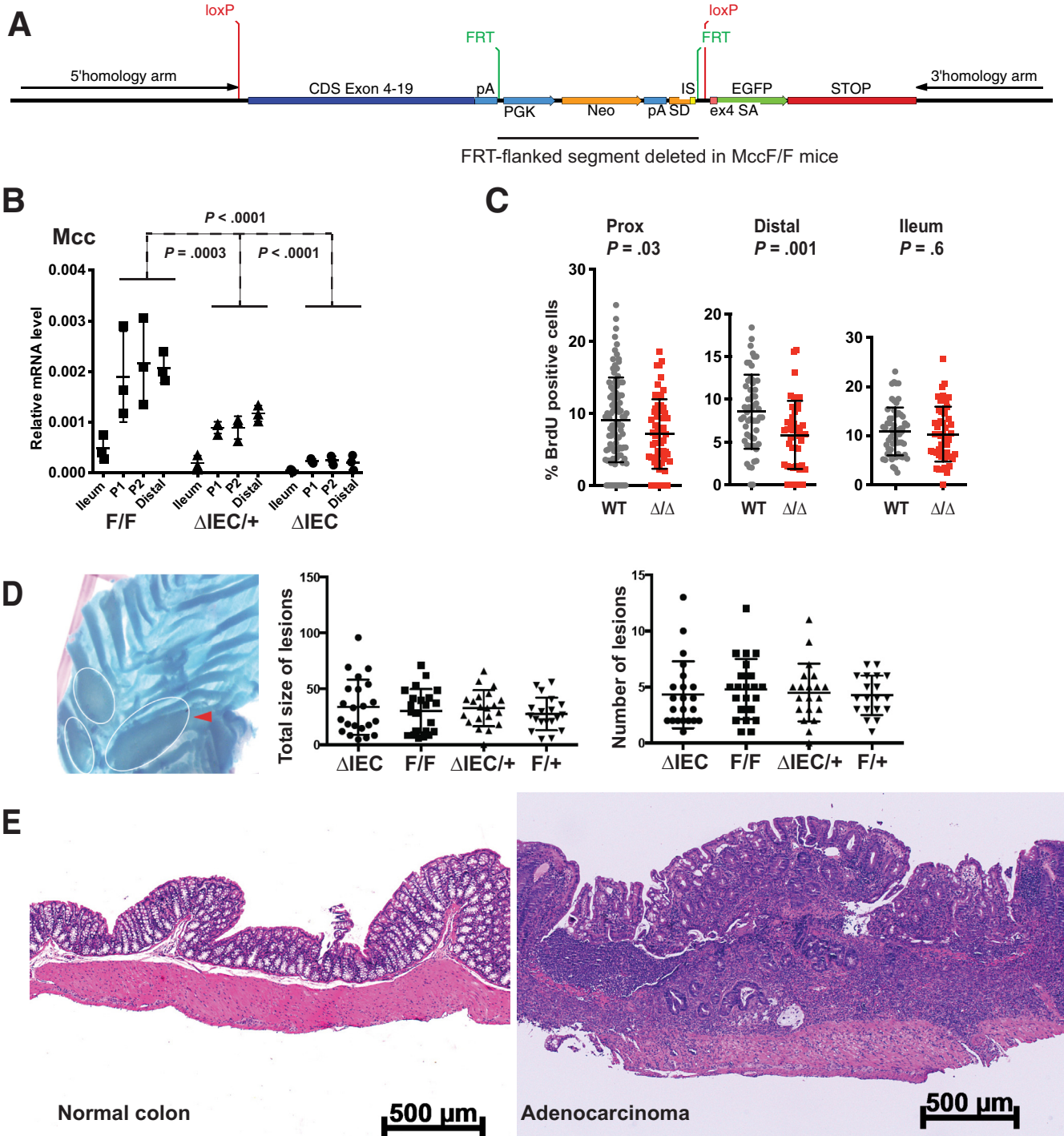
compared with matching normal tissue (Supplementary Tables 1–3). There were no significant differences between the genotypes for the most up-regulated genes listed in Table 1 (>12-fold in $Mcc^{\Delta IEC}$ mice) when the lesions of $Mcc^{F/F}$ and $Mcc^{\Delta IEC}$ mice were compared and data were corrected for multiple testing. Validation of selected genes was performed with quantitative polymerase chain reaction (qPCR) in different regions of the colon (Figure 2).

Many of the highly up-regulated genes identified in this study have been associated previously with inflammation or carcinogenesis[24,25] and were found in both $Mcc^{\Delta IEC}$ and $Mcc^{F/F}$ mice. They included S100A8/A9 (calprotectin), Mmp13 and other Mmps, Tgfβ, Tnfα, Cox2 (Ptgs2), the interleukin 1 family of cytokines (Ilβ, Ilα, Il33, Il1f9), and other inflammatory or immunosuppressive factors (Cxcl2/ Mip2, Il6, Cxcl1, Cxcl9, Cxcr2, Ido1, Pd-l1/Cd274), as well as the free radical nitric oxide–producing enzyme iNos2. Epithelial mesenchymal transition (EMT)-related factors included Tgm2, Hif1α, Plaur, Plau, Dcn, Hgf, Grem1, Vim, and Fn1. Gene set enrichment analysis (GSEA) of hallmark pathways[26] showed up-regulation of several inflammation and cancer-associated pathways (Table 2) that overlap with the mesenchymal subtype of colorectal cancer known as consensus molecular subtype 4 (CMS4).[27] The shared up-regulated pathways were EMT, inflammatory response, angiogenesis, complement, and transforming growth factor β signaling (Table 2).[27]

Another shared feature with CMS4 was the absence of β-catenin pathway hyperactivation in both genotypes. β-catenin target genes Lgr5 and Axin2 actually were down-regulated in the lesions compared with matching normal tissue from control-fed mice (Figure 2), similar to our previous report in Hif1α-deficient and WT mice.[18] Lgr5 expression is a key marker of colon stem cells[28,29] and loss of these cells was reported previously in dextran sodium sulfate (DSS)-induced colitis.[30] The cancers showed no evidence of β-catenin nuclear localization and both E-cadherin and β-catenin staining was strong in the membrane of the cancer cells in Mcc-expressing and Mcc-deficient mice (Figure 3A–D). Thus, cancer in this model is not driven by β-catenin hyperactivation, and down-regulation of Lgr5

expression suggests loss of colon stem cells and lack of regenerative potential in the inflammatory lesions.

Among the few highly down-regulated genes were Cyp2c67, Cyp2c68, Cyp2c40, and Cyp2c69 (5- to 12-fold) from the cytochrome P450 cluster on chromosome 19, which are orthologues of the human drug response gene CYP2C9. Expression of aryl hydrocarbon receptor (Ahr), another important drug response gene, was not altered in the lesions. However, there was an increase of cytoplasmic aryl hydrocarbon receptor (AHR) protein expression in the normal-appearing colon epithelium, which is known to absorb sulindac and its metabolites (Figure 3E–G).[16]

Inflammation Is Associated With Suppression of DNA Repair Pathways in Mcc-Deficient Mice

Although strong cancer-promoting genes and pathways were highly activated in the colonic lesions of both genotype groups (Tables 1 and 2), only 19% of Mcc-expressing controls developed cancer compared with 59% of Mcc-deficient mice. A significant difference between the 2 genotypes was in signatures of DNA repair, DNA replication, and cell-cycle regulation. GSEA analysis showed that the hallmark pathways G2M checkpoint, E2F targets, Myelocytomatosis oncogene cellular homolog (MYC) targets, and DNA repair were down-regulated in the lesions of Mcc-deficient mice compared with the lesions of Mcc-expressing mice (Table 2). This is consistent with the previously identified role of MCC in the DNA damage response.[8]

Further analysis of the DNA repair pathway data identified 29 genes that were down-regulated significantly in the lesions of Mcc-deficient mice (Figure 4A). These included the DNA mismatch repair (MMR) genes Msh3, Msh2, Mlh1, Mlh3, and Pms2. The baseline expression levels of MMR genes were similar between different regions of the colon within each group of control-fed mice (Figure 2). Msh2 expression was slightly higher in the colon of control-fed $Mcc^{\Delta IEC}$ mice than in Mcc-expressing mice. We analyzed the lesions and cancers for microsatellite instability (MSI) of mononucleotide repeats, a known marker of complete MMR deficiency,[31,32] but no instability was found (data not

Figure 1. (*See previous page*). **MCC deficiency drives inflammation-associated cancer but does not increase sulindac-induced macroscopic tissue damage in the mouse colon.** (A) The Mcc targeting vector construct was used to generate the $Mcc^{F/F}$ mouse line (B6.Cg-Mcc<tm1Maija>/Ausb). In cre-expressing mice, 2 truncated transcripts are expected; one includes Mcc exons 1–3 of the Mcc-201 isoform and the second includes Mcc exon 1 of the Mcc-202 isoform. (B) Significant reduction of full-length Mcc expression in the colon mucosa harvested from $Mcc^{\Delta IEC}$ (ΔIEC) and $Mcc^{\Delta IEC/WT}$ (ΔIEC/+) mice compared with $Mcc^{F/F}$ (F/F) mice, as determined by triplicate qPCR. A 2-tailed unpaired t test was used to determine statistical significance. Three mice were analyzed for each colon region. Error bars indicate the means with SD. (C) The percentage of proliferating, BrdU-positive, epithelial cells is reduced in $Mcc^{\Delta/\Delta}$ (Δ/Δ) mouse colon crypts compared with their WT siblings. A 2-tailed unpaired t test was used to determine statistical significance. Three mice/group and 20 crypts/mouse were analyzed. Error bars indicate the means with SD. (D) The number and size of drug-induced inflammatory lesions were similar in $Mcc^{\Delta IEC}$, $Mcc^{\Delta IEC/WT}$, $Mcc^{F/F}$, and $Mcc^{F/WT}$ (F/+) mice. Image shows the macroscopic appearance of the drug-induced lesions in methylene blue–stained tissue (circles and arrow), in a section of the proximal colon containing the V-shaped folds. Each dot represents the number and total area of lesions for a single mouse; 19–22 mice/group were analyzed. A 2-tailed unpaired t test with equal SD was used to determine statistical significance. Error bars indicate the means with SD. (E) H&E image of an adenocarcinoma harvested from a $Mcc^{\Delta IEC}$ mouse exposed to sulindac (right) and matching normal colon from a control-fed mouse (left). Original magnification, ×50. CDS, coding sequence; dist, distal colon mucosa; EGFP, Enhanced Green Fluorescent Protein; FRT, Flippase Recombinase Target; loxP, Locus of Crossover in P1; Neo, neomycin; pA, poly-A; PGK, Phosphoglycerate kinase; P1, P2, proximal colon mucosa; SA, splice acceptor site; SD, splice donor site.

Table 1. Altered Expression of the Most Highly Affected Genes Is Similar in Drug-Induced Colon Lesions of MCC[ΔIEC] and MCC[F/F] Mice

Gene symbol and name	Direction	Absolute fold change[a] MCC[ΔIEC]	Absolute fold change[a] MCC[F/F]
Mptx1; mucosal pentraxin 1	Down	184.9	90.4
S100a8; calgranulin A	Up	176.9	59.4
Mmp13; matrix metallopeptidase 13	Up	165.5	93.6
Il1b; interleukin 1β	Up	134.9	64.8
Il1a; interleukin 1α	Up	122.4	62.4
LincRNA identified by NONCODE; TC1300000114.mm.1[b]	Up	109.7	54.8
S100a9; calgranulin B	Up	106.7	29.1
Mptx2; mucosal pentraxin 2	Down	101.2	45.3
Mmp10; matrix metallopeptidase 10	Up	87.6	46.6
Ptgs2; prostaglandin-endoperoxide synthase 2	Up	74.2	38.4
Retnlg; resistin-like γ	Up	60.4	10.4
Gp49a; glycoprotein 49 A	Up	56.9	17.9
Lilrb4; leukocyte Ig-like receptor, subfamily B, member 4	Up	47.8	17.8
Clec7a; C-type lectin domain family 7, member a	Up	46.0	26.0
Cxcl9; chemokine (C-X-C motif) ligand 9	Up	41.9	54.6
Irgb6; Tgtp2, T-cell–specific GTPase 2	Up	30.6	35.7
Stfa2l1; stefin A2 like 1	Up	28.6	9.0
Nos2; nitric oxide synthase 2, inducible	Up	25.2	17.5
Cxcl2; chemokine (C-X-C motif) ligand 2, Mip2	Up	24.8	8.4
Steap4; STEAP family member 4	Up	23.6	15.3
Olr1; oxidized low density lipoprotein (lectin-like) receptor 1	Up	23.2	4.8
Gbp2; guanylate binding protein 2	Up	23.0	18.6
Irga family member; F830016B08Rik	Up	22.2	17.5
Ly6c2; lymphocyte antigen 6 complex, locus C2	Up	21.4	17.4
Tgm3; transglutaminase 3, E polypeptide	Down	20.9	16.1
Mmp12; matrix metallopeptidase 12	Up	19.9	8.2
F3; coagulation factor III	Up	19.4	11.2
Mrgpra2a; MAS-related GPR, member A2A	Up	19.0	4.0
Irg1; immunoresponsive gene 1	Up	18.5	6.6
Irga6; Iigp1, interferon inducible GTPase 1	Up	17.8	21.3
Dcn; decorin	Up	17.3	13.6
Il1f9; interleukin 1 family, member 9	Up	17.3	5.0
Akt3; thymoma viral proto-oncogene 3	Up	17.2	19.5
Reg3b; regenerating islet-derived 3 β	Up	16.9	28.7
Igsf6; immunoglobulin superfamily, member 6	Up	16.7	9.2
Reg3g; regenerating islet-derived 3 γ	Up	16.7	22.1
Sema3e; semaphorin 3E	Up	16.2	6.7
Irgm3; Igtp, interferon γ induced GTPase	Up	15.9	15.2
LincRNA identified by NONCODE; TC0700002949.mm.1	Up	15.3	4.6
LincRNA identified by NONCODE; TC1800000456.mm.1	Up	15.1	21.0
LincRNA identified by NONCODE; TC1900000899.mm.1	Up	15.1	6.8
Clec4e; C-type lectin domain family 4, member e	Up	15.0	5.4
Irgb family member; Gm12185	Up	14.3	16.5
Osmr; oncostatin M receptor	Up	13.9	9.5
Il33; interleukin 33	Up	13.6	5.4
NcRNA identified by NONCODE; TC0700004005.mm.1	Up	13.3	10.3
Il1rl1; interleukin 1 receptor-like 1	Up	13.3	9.1
Plek; pleckstrin	Up	13.3	5.4
Irgb10; Gm12250	Up	13.1	15.7

Table 1. Continued			
Gene symbol and name	Direction	Absolute fold change[a] MCC$^{\Delta IEC}$	Absolute fold change[a] MCC$^{F/F}$
Ifi204; interferon activated gene 204	Up	12.8	7.3
Sult1a1; sulfotransferase family 1A, phenol-preferring, member 1	Down	12.8	14.4
Ms4a4c; membrane-spanning 4-domains, subfamily A, member 4C	Up	12.8	10.6
Gm10720; predicted gene 10720	Up	12.7	3.0 (NS)
Mnda; myeloid cell nuclear differentiation antigen	Up	12.7	8.2
Cyp2c68; cytochrome P450, family 2, subfamily c, polypeptide 68	Down	12.6	12.4
Ly6c1; lymphocyte antigen 6 complex, locus C1	Up	12.3	11.9
Sequence 49 from patent WO2005040187	Up	12.2	5.1
Gpr110; G-protein–coupled receptor 110	Up	12.2	13.0
Ly6g; lymphocyte antigen 6 complex, locus G	Up	12.1	9.8
Adm; adrenomedullin	Up	12.0	4.7

NOTE. The genes are ranked according to the absolute fold-change of expression (>12-fold) in the lesions vs matching normal tissue in MCC$^{\Delta IEC}$ mice. The range of significant Q values for these genes is 1.7×10^{-11}-0.0001 (complete data are shown in Supplementary Tables 1, 2, and 3).
[a]Fold change compared with control-fed mice of the matching genotype, with a significant Q value (<0.05).
[b]Affymetrix probe set ID.

shown). This may indicate impairment but not a complete deficiency of MMR.

A further 12 of the down-regulated genes were associated with the homologous recombination repair (HR) pathway, such as *Atm*, *Rpa2*, and *Rad*. This profile of gene expression indicates a generalized defect of DNA repair involving different types of DNA damage. To understand how a lack of MCC is disrupting the response to inflammation, we used H_2O_2 to mimic the inflammation-induced free radical generation in mouse embryo fibroblasts (MEFs) prepared from whole-body knockout $Mcc^{\Delta/\Delta}$ mice and their WT siblings. $Mcc^{\Delta/\Delta}$ and WT MEFs were treated with H_2O_2 for 1–6 hours and the cell lysates then were examined for RNA or protein expression of DNA repair genes and markers of the DNA damage response. Expression of *Msh3*, *Msh2*, *Mlh1*, and *Atm* was reduced significantly in $Mcc^{\Delta/\Delta}$ MEFs compared with WT cells with 4- or 6-hour H_2O_2 exposure (Figure 4*B*). The WT MEFS showed phosphorylation of the checkpoint kinase (CHK)1 and CHK2 after H_2O_2 addition. This is consistent with activation of DNA damage response via the serine/threonine–protein kinases ataxia telangiectasia and Rad3-related (ATR) and ataxia telangiectasia mutated (ATM) (Figure 4*C*). $Mcc^{\Delta/\Delta}$ MEFS also showed phosphorylation of CHK2, which may indicate additional signaling through other kinases apart from ATM.[33] In contrast, the ATR-related signaling pathway, which leads to phosphorylation of CHK1 and the repair of DNA single-strand breaks (SSBs), was markedly suppressed. MCC expression itself also was induced by H_2O_2 exposure in WT MEFs (Figure 4*C*).

Surprisingly, we identified an increase in cell-cycle S-phase in $Mcc^{\Delta/\Delta}$ cells treated with H_2O_2 for 1–6 hours. There was also a sustained S-phase in cells allowed to recover in fresh medium after a 2-hour H_2O_2 exposure (Figure 4*D*). This led us to ask whether the increase in S phase after the DNA damage associated with MCC loss was owing to an active or arrested S-phase. We performed Western blot for the key cell-cycle regulator retinoblastoma (RB) and phosphorylated RB as a measure for an active S-phase. The WT MEFs responded to H_2O_2 with a loss of phosphorylation of RB within 1 hour. By contrast, $Mcc^{\Delta/\Delta}$ MEFS showed sustained, or a slight increase in, phosphorylation of phosphorylated RB after exposure to H_2O_2 (Figure 4*C*). Consequently, it appears that there is loss of DNA damage response signaling in $Mcc^{\Delta/\Delta}$ MEFS that may be accompanied by sustained proliferation. To confirm these observations, we analyzed whether MCC loss also leads to a relative increase of S-phase in UV-treated HCT116 cells, which express endogenous MCC (Figure 4*D*). Both non-targeted (NT) and MCC-knockdown (KD) cells showed a subtle increase in S-phase 24 hours after 10 J/m^2 UV treatment. However, the MCC-KD cells showed a trend for a more persistent increase in S-phase fraction at 48 hours that continued until 72 hours after treatment.

Exposure to mutagens during an active S-phase means that there is a greater likelihood that the cells sustain DNA damage, which then may be integrated into the genome through low-fidelity repair mechanisms. To test whether MCC-knockdown cells sustain greater DNA damage in S-phase, we subsequently treated HCT116 cells with SN38, which is a metabolite of the chemotherapy drug irinotecan and causes SSBs. A comet assay showed that MCC-knockdown cells have greater DNA damage compared with NT cells after treatment with SN38 (Figure 4*E*). DNA damage also was increased in H_2O_2-treated $Mcc^{\Delta/\Delta}$ MEFS with defective CHK1 signaling. There was a strong increase of gamma histone 2AX (γH2AX), whereas in WT MEFs the increase was minimal (Figure 4*C*). γH2AX is a marker of double-strand break damage that can develop from SSB through DNA replication when SSB repair is deficient. Thus, a lack of MCC can lead to an increase in both SSB and double-strand break damage.

Msh2

Msh3

Axin2

Lgr5

Cyp2c68

Mcc

Mmp13

Mmp10
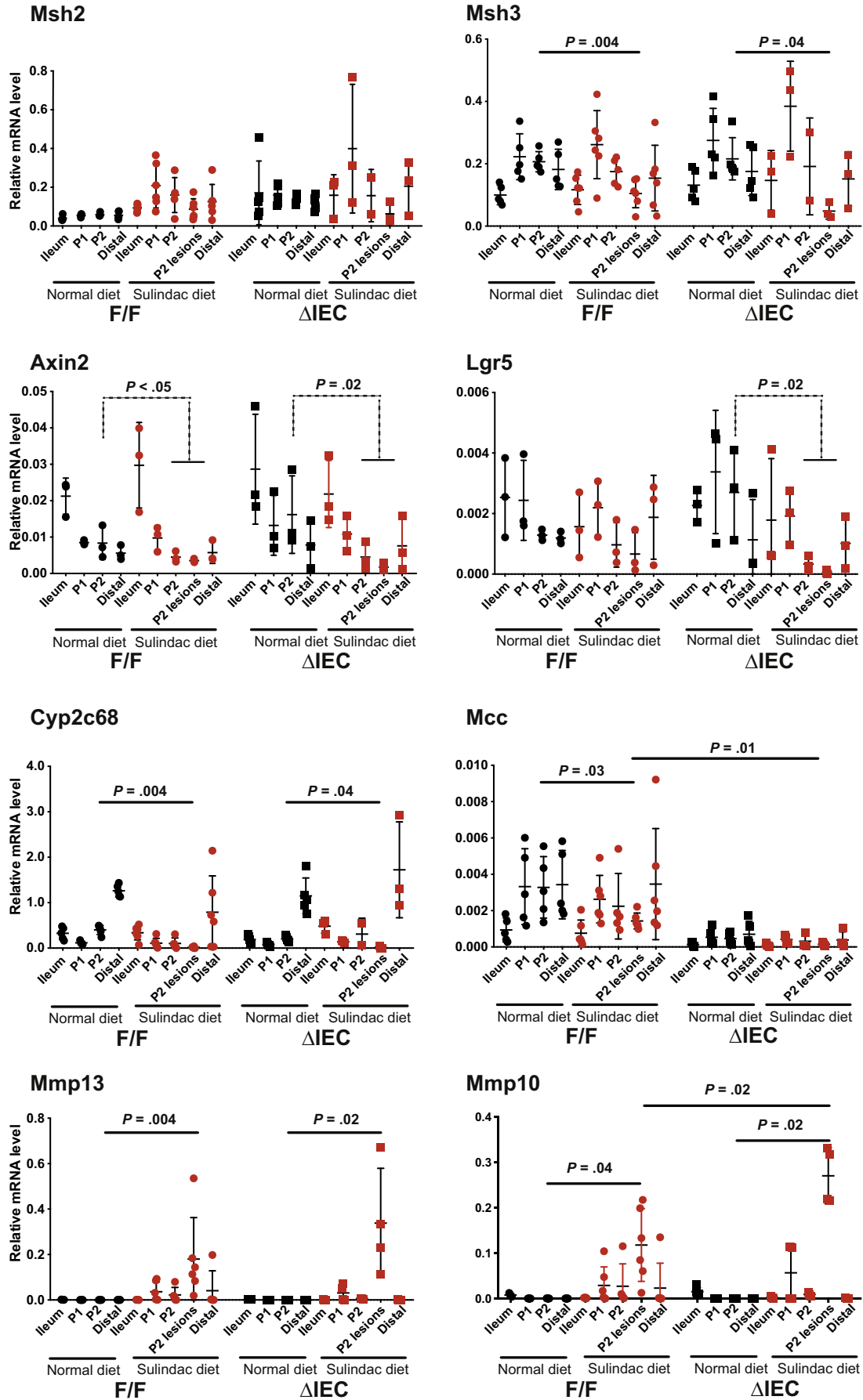
Drug-Induced Lesions Show a Strong Interferon γ–Induced Guanosine Triphosphatase Response to Colon Barrier Destruction

Because the impact of *Mcc* deficiency on carcinogenesis was shown only in the drug-induced lesions, we proceeded to investigate if sulindac-induced colon inflammation is similar or has some unique features compared with another model of colon inflammation. Search of the literature for a comparable gene profiling study identified a report on DSS colitis that develops in the mouse mid-distal colon.[34] The gene profiles were strikingly similar between the 2 models, although the time scale of drug exposure was different, 6 days of DSS vs 10 weeks of sulindac (Figure 5A). Overall, the 2 studies were correlated positively (r = 0.55; P < 2e-16) and 1602 differentially expressed probe sets were highly correlated (r = 0.82). This is compatible with the concept that both models involve colon barrier destruction.

The top 2 GSEA hallmark pathways[26] activated in our study were interferon γ (IFNγ) response and EMT (Table 2). These indicate strong responses to colon barrier destruction and bacterial invasion of the underlying tissue layers.[25,35] A prominent feature of the colon lesions in both genotype groups was the induction of at least 28 IFNγ-induced guanosine triphosphatase (GTPase) genes, usually thought to be associated with the host response to external pathogens and not previously recognized in the mouse colon. Several clusters of these genes were identified on chromosomes 3, 5, 7, 11, and 18, which also included long noncoding RNAs (Table 3).[36] Sixteen of the up-regulated genes represent the *Irg* (p47-GTPase) subfamily, of which only the *IRGM* and *IRGC* genes have been retained through evolution in human beings. *IRGM* is a candidate for the Crohn's disease susceptibility locus.[37] We identified only 11 IFNγ-induced GTPase genes in the previous generation Affymetrix array (Santa Clara, CA) used for the DSS colitis study, but most of them also were up-regulated in that study (Figure 5A). Therefore, up-regulation of IFNγ-induced GTPases is not unique to sulindac-induced colon inflammation.

Two of the genes *Irga6* (*Iigp1*) and *Irgb6* (*Tgtp2*) were selected for validation by qPCR in different parts of the colon. The level of expression was variable but was increased in the sulindac-induced lesions (Figure 5B). To investigate the possibility that the high expression of these genes was related to an undetected pathogen infection in the animals, we analyzed colon specimens from 3 experiments over 4 years and found that *Irgb6* and *Irga6* genes were consistently up-regulated in sulindac-induced lesions, similar to the chemokine *Mip2* (Figure 5C). We then treated CT26 mouse colon cancer cells in vitro with lipopolysaccharide, a component of the bacterial membrane. This treatment also induced the expression of *Irgb6*, *Irga6*, and *Mip2* (Figure 6A), similar to the induction of

proinflammatory signaling shown previously in vitro by sulindac sulfide.[17,18] Therefore, the strong expression of multiple IFNγ-induced GTPases is a previously unrecognized feature of mouse colitis that is not necessarily related to an external pathogen infection, but can be triggered by gut bacteria invading the submucosa and causing inflammation after sulindac-induced initial injury. Proinflammatory factors also can induce the same response in vitro.

We analyzed the protein expression of 2 of the highly up-regulated genes *Irga6* and *Irgm3*. There was no expression of Immunity-related GTPase A6 (IRGA6) in the normal colon of drug-treated or untreated mice, but it was present in most of the lesions. There was strong cytoplasmic expression in the mesenchymal cells, such as fibroblasts/myofibroblasts and macrophages, in the areas of acute inflammation associated with erosions or ulceration of the mucosa (Figure 6). There was also strong cytoplasmic expression of enterocytes in the colonic epithelium at the edges of these areas of ulceration, but very weak expression in the cancer cells. There was no expression of IRGA6 in the lymphocytes or neutrophils in the inflamed tissue. Immunity-related GTPase M3 (IRGM3) expression also mostly was absent in the normal colon apart from isolated plasma cells and endothelium of blood vessels. Inflammation induced IRGM3 expression in the colonic epithelium and also was seen in infiltrating plasma cells and macrophages (Figure 6). Similar patterns of IRG protein expression were found in both $Mcc^{\Delta IEC}$ and $Mcc^{F/F}$ mice.

Discussion

This study shows that loss of MCC expression promotes inflammation-associated cancer in the mouse colon. Despite a strong cancer-promoting phenotype in the inflamed tissue in both genotypes, only 19% of the genotype controls ($Mcc^{F/F}$) developed malignant tumors, compared with 59% of the $Mcc^{\Delta IEC}$ mice. The background cancer frequency is comparable with WT mice exposed to sulindac (5%–16%)[16,18] or DSS (17%–22%).[38] The gene profiles in the inflamed tissue showed a much wider spectrum of the signaling pathways than previously recognized, including novel coding and noncoding genes. The data implicate activation of cancer-promoting genes and pathways in producing a premalignant tissue microenvironment, which does not involve β-catenin hyperactivation. We found that β-catenin protein expression was mainly localized in the epithelial cell membrane in the tumors. The lack of nuclear β-catenin hyperactivity was shared by both $Mcc^{F/F}$ and $Mcc^{\Delta IEC}$ mice in our study and is similar to the mesenchymal CMS4 subtype in human beings, which may comprise up to 23% of colorectal cancers.[27] There are also other important similarities between sulindac-induced inflammation and

Figure 2. (*See previous page*). **Validation of altered gene expression in inflammatory lesions.** The mucosal lining was harvested from ileum, proximal P1 and P2, proximal P2 lesions, and distal colon of mice given either sulindac or the control diet (3–6 mice/group). In sulindac-fed mice, P2 refers to macroscopically normal-appearing tissue adjacent to the visible lesions. RNA expression was analyzed by triplicate qPCR and normalized to *Gapdh*. P values are shown only for the differences in the P2 region. A 2-tailed Mann–Whitney test was used to determine statistical significance. Error bars indicate the means with SD. mRNA, messenger RNA.

Table 2. Hallmark Pathways for DNA Repair, G2M Checkpoint, MYC Targets and E2F Targets Are Up-regulated in *Mcc*^F/F Mouse Lesions but Down-regulated in *Mcc*^ΔIEC Mouse Lesions (shown in bold)

GSEA hallmark pathway	ES MCC^F/F lesions vs normal tissue	FDR Q value	ES MCC^ΔIEC lesions vs normal tissue	FDR Q value	ES MCC^ΔIEC vs MCC^F/F lesions vs lesions	FDR Q value
Inflammation and cancer						
Interferon γ response	0.80	0	0.78	0	0.31	0.004
Epithelial mesenchymal transition	0.77	0	0.78	0	0.57	0
Allograft rejection	0.76	0	0.75	0	0.47	0
Interferon α response	0.80	0	0.77	0	0.24	0.29 NS
Inflammatory response	0.69	0	0.74	0	0.57	0
IL6 JAK STAT3 signaling	0.76	0	0.78	0	0.61	0
TNFα signaling via NF-κB	0.68	0	0.75	0	0.71	0
Angiogenesis	0.68	0	0.77	0	0.53	0
TGFβ signaling	0.57	0	0.62	0	0.55	0
Apical junction	0.54	0	0.61	0	0.42	0
Apical surface	0.59	0	0.54	6.84E-04	0.32	0.097 NS
Apoptosis	0.56	0	0.59	0	0.46	0
KRAS signaling up	0.55	0	0.61	0	0.47	0
IL2 STAT5 signaling	0.55	0	0.58	0	0.43	0
Hypoxia	0.51	0	0.60	0	0.52	0
Complement	0.62	0	0.66	0	0.49	0
Coagulation	0.60	0	0.66	0	0.49	0
PI3K Akt mTOR signaling	0.44	7.8E-04	0.38	0.017	0.23	0.260 NS
DNA damage and checkpoints						
G2M checkpoint	**0.53**	**0**	**-0.30**	**0.093 NS**	**-0.62**	**0**
DNA repair	**0.18**	**0.94 NS**	**-0.39**	**0.008**	**-0.45**	**0**
Mitotic spindle	0.48	0	0.36	0.013	-0.27	0.043
UV response down	0.47	0	0.51	0	0.37	4.1E-04
Cell cycling and cell growth						
MYC targets v1	**0.66**	**0**	**-0.34**	**0.024**	**-0.70**	**0**
MYC targets v2	**0.52**	**1.8E-04**	**-0.40**	**0.037**	**-0.72**	**0**
E2F targets	**0.55**	**0**	**-0.48**	**0**	**-0.73**	**0**
Metabolism						
mTORC1 signaling	0.56	0	0.39	0.004	-0.34	6.0E-04
Unfolded protein response	0.43	9.7E-04	-0.25	0.494 NS	-0.50	0
Adipogenesis	-0.37	0.004	-0.45	0	-0.36	4.5E-04
Fatty acid metabolism	-0.45	0	-0.52	0	-0.40	1.6E-04
Peroxisome	-0.47	0	-0.49	0	-0.29	0.075 NS
Oxidative phosphorylation	-0.40	0.001	-0.66	0	-0.66	0

NOTE. Positive ES (maximum, 1) indicates up-regulation of pathway and negative values show down-regulation. Hallmark pathways for G2M checkpoint, DNA repair, MYC targets v1, MYC targets v2 and E2F targets are down-regulated in *Mcc*^ΔIEC lesions compared to *Mcc*^F/F lesions.

ES, enrichment score; FDR, false discovery rate; IL, interleukin; JAK, Janus kinase; mTOR, Mechanistic Target of Rapamycin Kinase; NF-κB, nuclear factor-κB; PI3K, Phosphoinositide 3-kinase; STAT, Signal Transducers and Activators of Transcription; TGF, transforming growth factor.
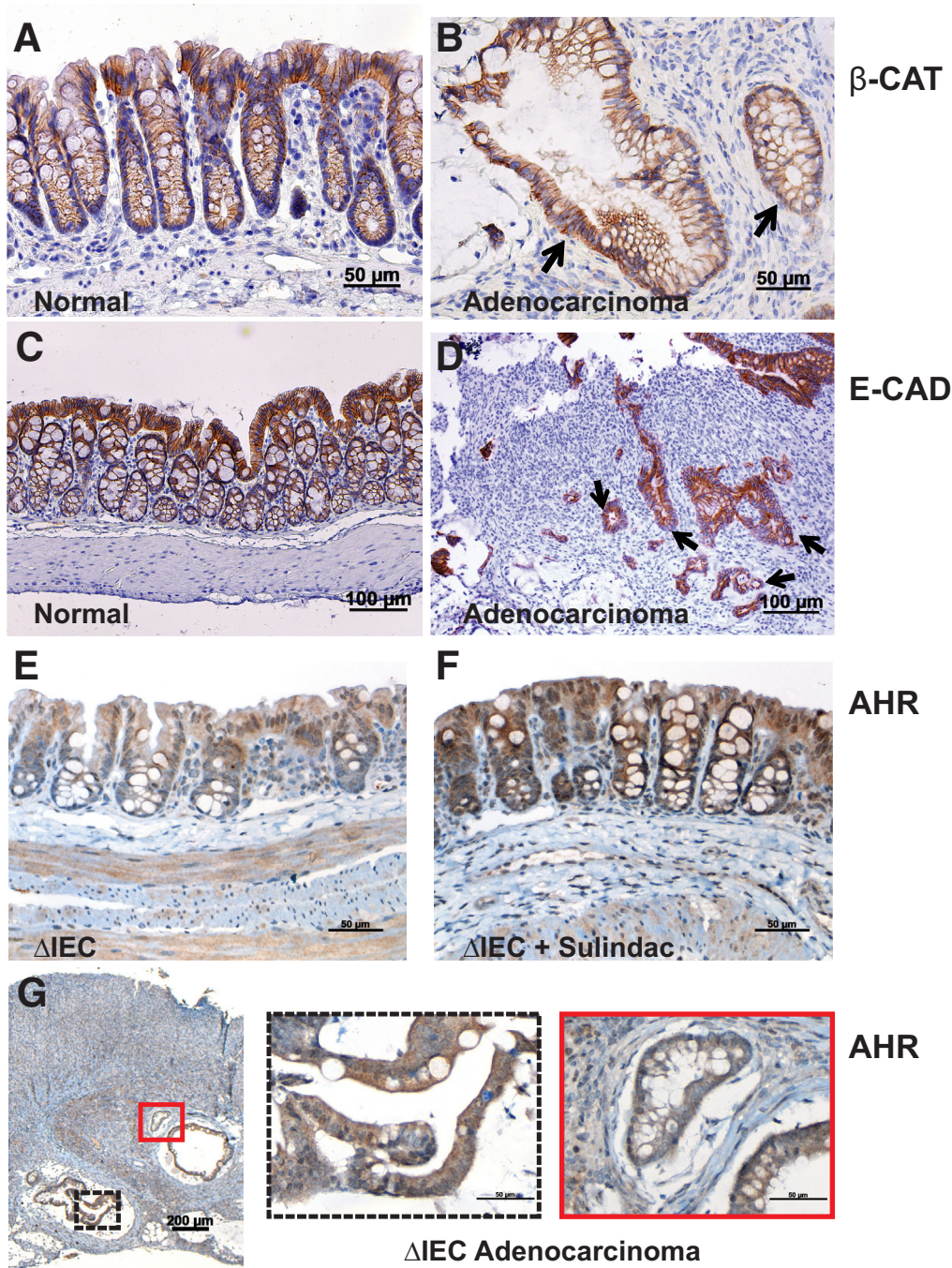
Figure 3. Tissue expression of β-catenin, E-cadherin, and AHR in the inflamed mouse colon and cancers. (*A* and *B*) Cancer cells maintain strong membranous β-catenin (β-CAT) expression. (*arrows*). (*C* and *D*) Cancer cells maintain E-cadherin (E-CAD) expression (*arrows*). (*E–G*) AHR was expressed diffusely in the cytoplasm of normal colonic epithelium and was increased in mice exposed to sulindac. AHR expression was present in the inflammation-associated adenocarcinoma. Original magnification: (*A, B, E, F, G inset*) ×400, (*C* and *D*) ×200, and (*G*) ×100.

CMS4 because many of the up-regulated gene expression pathways are the same (EMT, Inflammatory Response, Angiogenesis, Complement and TGF Beta Signaling). In addition, down-regulation of MYC target genes is characteristic for both $Mcc^{\Delta IEC}$ mouse lesions and CMS4.

Loss of MCC causes a slight decrease in epithelial cell proliferation in the normal colon, which could be related to a small impairment of the DNA damage response to a background level of DNA SSBs occurring in the healthy colon, but has no significant phenotypic effect in the adult mouse or during development.[39] In stressed inflammatory conditions a lack of MCC causes subtle but widespread down-regulation of pathways involved with DNA damage and replication, such as the G2M checkpoint and DNA repair (Table 2). In the same conditions, MCC-expressing mice showed up-regulation of these pathways. This up-regulation is a normal response to DNA damage and replication stress caused by reactive oxygen and nitrogen species, which are generated by the inflammation.[40] Oxidative stress itself also is known to impair MMR protein function, which is thought to cause low-level MSI associated with chronic inflammation.[41] The gene expression changes observed here were
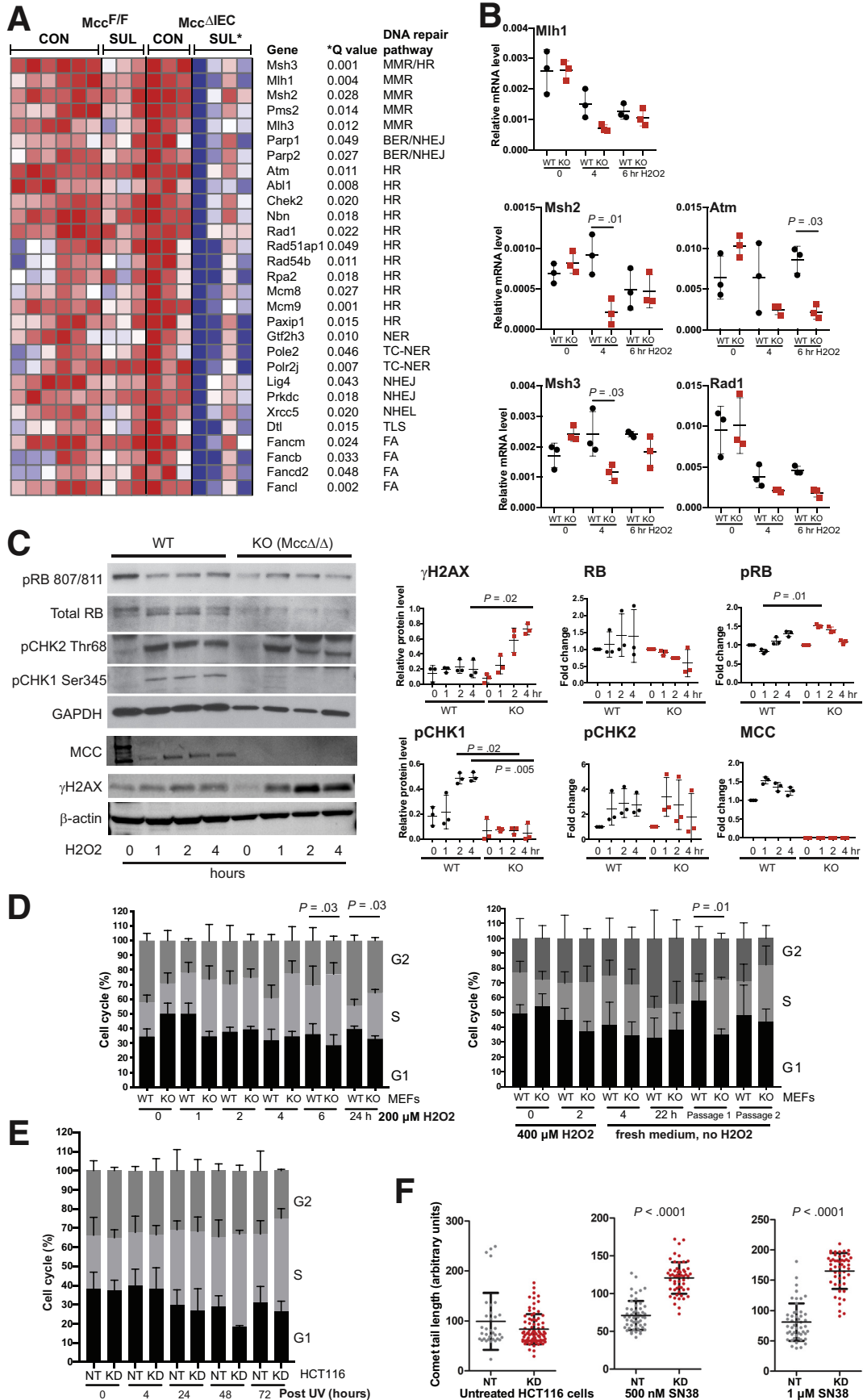
associated primarily with *Mcc* deletion in the inflamed colon tissue. It remains to be determined whether *MCC* silencing contributes to the MSI-low phenotype in chronic IBD. Complete MMR deficiency also can cause a loss of the G2/M checkpoint after *N*-methyl-*N'*-nitro-*N*-nitrosoguanidine or tioguanine-induced DNA damage.[42] However, it is unclear whether our observations in *Mcc^ΔIEC* mice are related to the same cellular process.

Curiously, we also observed down-regulation of E2F target genes by GSEA of *Mcc^ΔIEC* mice (Table 2). The E2F transcription factor family plays a central role in the sequential expression and repression of genes required for cell-cycle progression, DNA repair, and replication. For example, MMR and many other DNA repair genes are transcribed by E2F.[43] Sustained E2F activity is a key cellular mechanism to allow cells to recover from DNA damage induced by replication stress and is mediated by activation of CHK1.[44–46] Because we showed that the absence of MCC prevented the phosphorylation of CHK1 in MEF cells exposed to the DNA damaging agent H_2O_2, it is possible that the *Mcc^ΔIEC* mice failed to activate an E2F transcriptional cascade in response to excessive DNA damage and replication stress in the inflamed lesions. This suggests a role for MCC in the cell-cycle S-phase checkpoints that have evolved to respond to potential failures in DNA repair and replication. Defective E2F signaling contributes to genomic instability, a recognized hallmark of cancer.[47]

Our study also described a previously unrecognized feature of mouse colitis, coordinated up-regulation of 28 members of the IFNγ-induced GTPase superfamily that defends mammalian cells against a diverse group of invading pathogens, such as intracellular bacteria and protozoa.[48–51] Here, this up-regulation was seen in the absence of external pathogen involvement in the inflamed colon and was restricted to immediate proximity of the damaged epithelial barrier that allows translocation of the gut microbiome. This feature has become evident in our study by using the latest generation microarrays that provide a much wider coverage of the genome. In the mouse there are 3 highly complex subfamilies, *Irg*, *Gvin*, and *Gbp*, each with different roles and functions. They have not been linked with carcinogenesis, although other GTPases, such as *Ras*, *Rac*, and *Rho*, are well-known oncogenes and EMT promoters when mutated or up-regulated.

In the human colon, overexpression of a germline variant of the *IRGM* gene has been associated with susceptibility to Crohn's disease–associated chronic inflammation.[52,53] In the mouse, IRG protein activation is more complex with 2 groups of factors, the regulatory GMS (IRGM1–3) and the effector GSK subfamily (multiple IRGA and IRGB proteins), which have complementary roles. Expression of some of the IRG proteins has been characterized in vitro in the context of intracellular bacterial or parasite infections and activation of the NLRP3 inflammasome.[50] Further studies are required to determine the functional consequences of the concordant expression of the *Irg*/noncoding RNA clusters in the inflamed tissue and whether there is any similarity to the defect of intracellular bacterial clearance in Crohn's disease that increases inflammation.[52,53] It also is possible that the composition of the gut microbiome can affect the level of expression/activation of the IRG proteins and the severity of inflammation. It is well known that the severity and timing of experimental colitis can vary depending on the dosage and duration of drug exposure, mouse strain, housing conditions, and composition of the gut microbiome.[54] Therefore, these genes could be pursued further as potential markers of a pathogenic response to drug toxicity or severity of inflammation in the colon and its interplay with the gut microbiome.

It is likely that the strong inflammatory EMT and IFNγ response observed in the 10-week lesions was caused by colon barrier destruction. However, sulindac exposure clearly was the trigger, possibly by causing the initial drug toxicity and erosion of the surface mucosa through increased AHR signaling. Sulindac is a ligand of AHR and can cause proinflammatory AHR, nuclear factor-κB (NFκB), and AP-1 Transcription Factor Subunit cJUN (cJUN) signaling in vitro that is reversed when *AHR* is knocked down.[18,55] We

---

Figure 4. (*See previous page*). **MCC deficiency causes down-regulation of DNA repair genes in the inflamed colon and increases SSBs and double-strand breaks through compromised DNA damage signaling.** (*A*) Transcriptome analysis of sulindac drug-induced (SUL) lesions and the matching tissue from control-fed mice (CON). A subset of DNA repair genes was down-regulated significantly in the lesions of *Mcc^ΔIEC* mice. Low and high expressed genes in the heatmap are shown in blue and red, respectively. Genes were assigned to the corresponding DNA repair pathways: MMR, mismatch repair; BER, base excision repair; HR, homologous recombination repair; TC-NER, transcription coupled nucleotide excision repair; NHEJ, nonhomologous end-joining; TLS, translesion synthesis; and FA, Fanconi anemia pathway. Statistical significance was determined using limma via the limmaGP tool in GenePattern.[64] (*B*) *Mcc* deletion causes down-regulation of *Msh2*, *Msh3*, and *Atm* gene expression in MEFs treated with 400 μmol/L H_2O_2. The graphs show values from 3 independent experiments with the same MEF cell lines. RNA expression was analyzed by triplicate qPCR and normalized to *Gapdh*. Statistical significance between WT and knockout (KO) was determined using the 2-tailed Kruskal–Wallis test. Error bars indicate the means with SD. (*C*) MCC deficiency causes loss of Chk1-S345 phosphorylation and an increase of γH2AX and RB phosphorylation in MEFs treated with 400 μmol/L H_2O_2. The graphs show quantification of protein expression from 3 independent experiments. Statistical significance was determined using the 2-tailed Kruskal–Wallis test. Error bars indicate the means with SD. (*D* and *E*) MCC deficiency or KD causes an increase in cell-cycle S-phase in MEFs treated with 200 μmol/L H_2O_2 and in MEFs allowed to recover in fresh medium after a 2-hour H_2O_2 treatment (400 μmol/L), as well as in UV-treated HCT116 cells. Statistical significance was determined using the 2-tailed Mann–Whitney and Kruskal–Wallis tests (3–4 independent experiments). Error bars indicate means with SD. (*F*) SN38 treatment leads to higher levels of DNA damage in MCC-KD HCT116 cells than in NT vector control cells. Comets (N = 35–83) scored from 3 independent experiments were combined and plotted in a *dot plot*. Two-tailed unpaired *t* tests were performed (95% CI) to determine the statistical significance between the 2 groups. Error bars indicate the means with SD.

Figure 5. Gene expression profiles are similar between DSS colitis and sulindac-induced colon inflammation. (*A*) Global comparison of gene expression in sulindac-induced lesions (*Mcc^F/F* mice) with the DSS colitis data reported by Fang et al[34] in 2011. Log fold-change between the end points and controls were plotted for probe sets that were differentially expressed in both of the studies (blue, N = 1602), this study only (green, N = 702), or Fang et al[34] study only (pink, N = 5637). IFNγ-induced GTPases that were common for both studies are highlighted in black. A total of 10,957 probe sets that were not differentially expressed in either study were not plotted. (*B*) Validation of up-regulated *Irga6* and *Irgb6* expression in the inflammatory lesions (3–6 mice per group). RNA expression was analyzed by triplicate qPCR and normalized to *Gapdh*. A 2-tailed Mann–Whitney test was used to determine statistical significance. Error bars indicate the means with SD. (*C*) Expression of *Irga6*, *Irgb6*, and the chemokine *Mip2* (positive control of inflammation) in the lesions from 3 independent mouse experiments (3 mice/experiment; 3 technical replicates/lesion also shown). Lesions and proximal control tissue were analyzed from the same mice. *P* values are shown only for the differences in the P2 region. Gene expression was analyzed by qPCR, and normalized to *Gapdh* expression. A 2-tailed Wilcoxon matched-pairs signed-rank test was used to determine statistical significance. Error bars indicate the means with SD. Exp, Experiment; prox, proximal colon adjacent to lesions.

Table 3. Differential Expression of IFNγ–Induced GTPase Genes and Co-localizing ncRNAs in the Drug-Induced Colon Lesions From MCC[F/F] Mice, Compared With Matching Normal Tissue

Affymetrix ID	Fold[a]	Direction	Q value[b]	Chromosomal location[c]	Gene symbol or name
TC0700003994.mm.1	2.8	Down	0.048	7: 105,852,518–105,855,944	LincRNA identified by NONCODE
TC0700003996.mm.1	6.1	Up	3.4E-06	7: 105,895,118–105,953,970	VLIG1 (Gm4070)
TC0700003998.mm.1	2.5	Down	0.045	7: 106,076,751–106,084,046	VLIG1 pseudogene (Gm8979)
TC0700004000.mm.1	2.8	Down	0.048	7: 106,113,896–106,117,322	LincRNA identified by NONCODE
TC0700004002.mm.1	7.6	Up	4.2E-06	7: 106,156,556–106,215,326	Gvin1
TC0700004003.mm.1	6.7	Up	3.0E-06	7: 106,185,743–106,190,099	Gvin1 pseudogene (Gm18853)
TC0700004004.mm.1	5.5	Up	1.5E-05	7: 106,200,812–106,203,310	NcRNA identified by NONCODE
TC0700004005.mm.1	10.3	Up	6.4E-06	7: 106,207,673–106,210,791	NcRNA identified by NONCODE
TC1100002641.mm.1	3.1	Up	1.2E-07	11: 48,861,968–48,871,683	Irgm1 (Lrg47)
TC1100002642.mm.1	2.8	Up	7.7E-03	11: 48,887,422–48,902,152	Irgb8-b9 (Gm5431)
TC1100002643.mm.1	16.5	Up	5.4E-07	11: 48,904,656–48,994,172	Irgb1-b2 (Gm12185) and Irgb6* (Tgtp1)
TC1100004292.mm.1	3.1	Up	1.3E-04	11: 48,946,150–48,979,398	Irgb3-b5* (9930111J21Rik1)
TC1100002647.mm.1	2.8	Up	8.2E-04	11: 49,014,075–49,014,785	LincRNA identified by NONCODE
TC1100002648.mm.1	3.3	Up	1.0-E04	11: 49,015,874–49,051,242	Irgb4-b5 (9930111J21Rik2)
TC1100002649.mm.1	35.7	Up	6.6E-07	11: 49,057,194–49,064,212	Irgb6 (Tgtp2)
TC1100000496.mm.1	2.2	Up	2.12E-5	11: 48,978,889–49,135,387	Irgd (Ifi47; Irg47)
TC1100000681.mm.1	15.7	Up	1.9E-08	11: 58,183,843–58,190,198	Irgb10 (Gm12250)
TC1100004265.mm.1	15.2	Up	1.6E-07	11: 58,199,556–58,207,592	Irgm3 (Igtp)
TC1100004266.mm.1	3.5	Up	8.5E-06	11: 58,199,618–58,222,779	Irgm2 (Iigp2)
TC1100000683.mm.1	6.5	Up	1.5E-05	11: 58,202,415–58,204,772	NcRNA identified by NONCODE
TC1800000606.mm.1	11.3	Up	5.4E-07	18: 60,212,077–60,247,820	Irga2 (Gm4951)
TC1800000607.mm.1	9.9	Up	1.1E-05	18: 60,220,843–60,222,058	Irga8 (Gm5970)
TC1800000608.mm.1	3.3	Up	2.8E-05	18: 60,257,748–60,288,497	NcRNA identified by NONCODE
TC1800001396.mm.1	10.5	Up	1.5E-05	18: 60,268,301–60,273,267	Irga3 (Gm4841)
TC1800000609.mm.1	17.5	Up	1.0E-05	18: 60,293,380–60,303,016	Irga4 (F830016B08Rik)
TC1800000610.mm.1	21.3	Up	2.3E-07	18: 60,376,028–60,392,634	Irga6 (Iigp1)
TC0300001444.mm.1	3.8	Up	6.5E-06	3: 142,493,978–142,522,344	Gbp5
TC0300001445.mm.1	8.8	Up	5.2E-07	3: 142,530,342–142,550,149	Gbp7
TC0300001446.mm.1	4.2	Up	2.0E-06	3: 142,560,026–142,573,209	Gbp3
TC0300001447.mm.1	18.6	Up	1.9E-07	3: 142,620,602–142,638,008	Gbp2
TC0500003729.mm.1	5.0	Up	9.9E-05	5: 105,014,150–105,139,540	Gbp8
TC0500003730.mm.1	5.3	Up	1.5E-05	5: 105,077,630–105,139,539	Gbp9
TC0500003731.mm.1	7.7	Up	4.1E-06	5: 105,115,767–105,139,586	Gbp4
TC0500002895.mm.1	8.1	Up	3.1E-06	5: 105,215,699–105,239,533	Gbp10
TC0500002896.mm.1	3.8	Up	4.3E-05	5: 105,323,042–105,346,472	Gbp11

NOTE. Gene nomenclature is from Lilue et al.[36]
LincRNA, Long intergenic non-coding RNA; LncRNA, Long non-coding RNA.
[a]Fold-change in sulindac-fed mice compared with control-fed mice.
[b]Q value is the significance corrected for multiple comparisons.
[c]Genomic coordinates from Mouse Genome Assembly GRCm38.p4.

showed previously that small lesions become visible and show up-regulation of NFκB target genes after 1 week of sulindac exposure.[16,17] The tissue toxicity caused by nonsteroidal anti-inflammatory drugs (NSAID) is well documented in the human gastrointestinal tract.[56] A germline variant of CYP2C9 causes low activity of the enzyme and susceptibility to NSAID–associated gastrointestinal bleeding.[57] We observed a coordinated decrease in the expression of the drug response gene cluster *Cyp2c67*, *Cyp2c68, Cyp2c40*, and *Cyp2c69*, which are orthologues of

human CYP2C9. Down-regulation of these genes also was found in DSS colitis[34] and thus may be more widely associated with drug-induced colon barrier destruction rather than being a sulindac-specific alteration.

This study has shown widespread similarities in the gene expression profiles of sulindac and DSS-induced colitis. Furthermore, similar to the azoxymethane/DSS model of colon cancer, male mice are more susceptible than female mice to cancer associated with sulindac-induced inflammation.[58] Although DSS colitis typically is diffuse and more
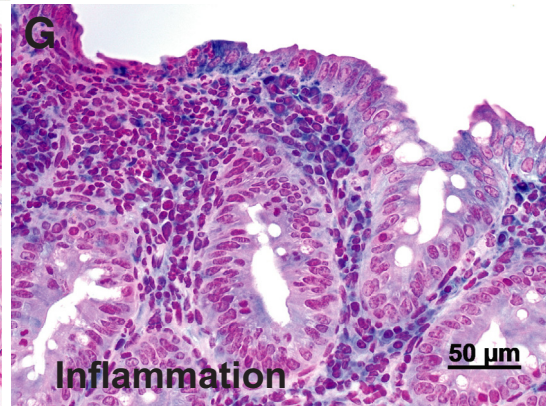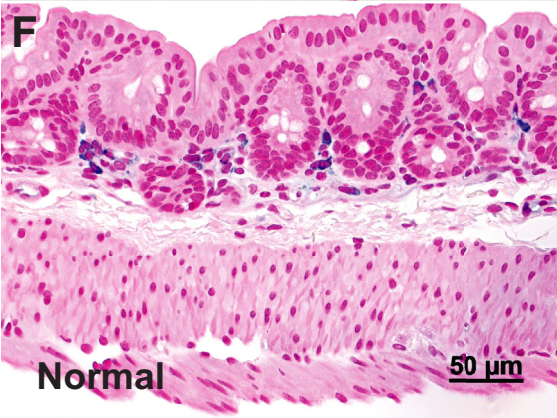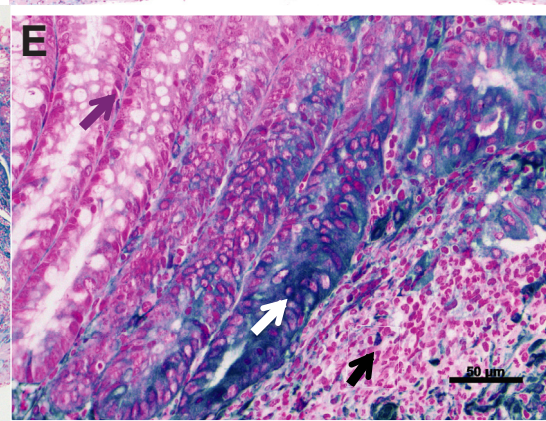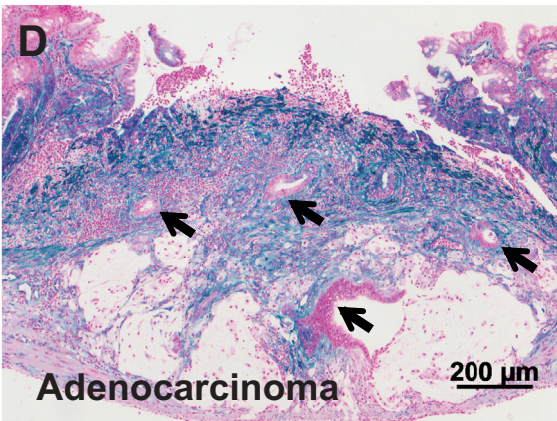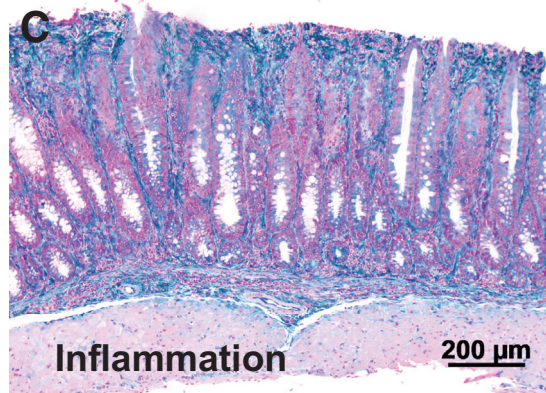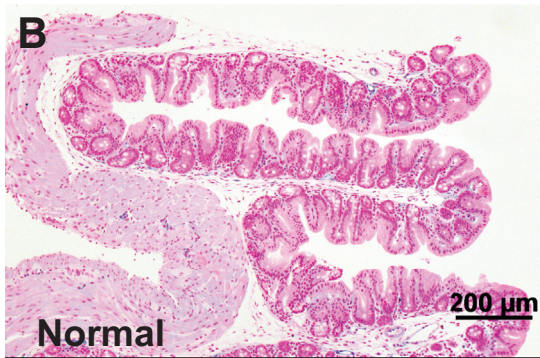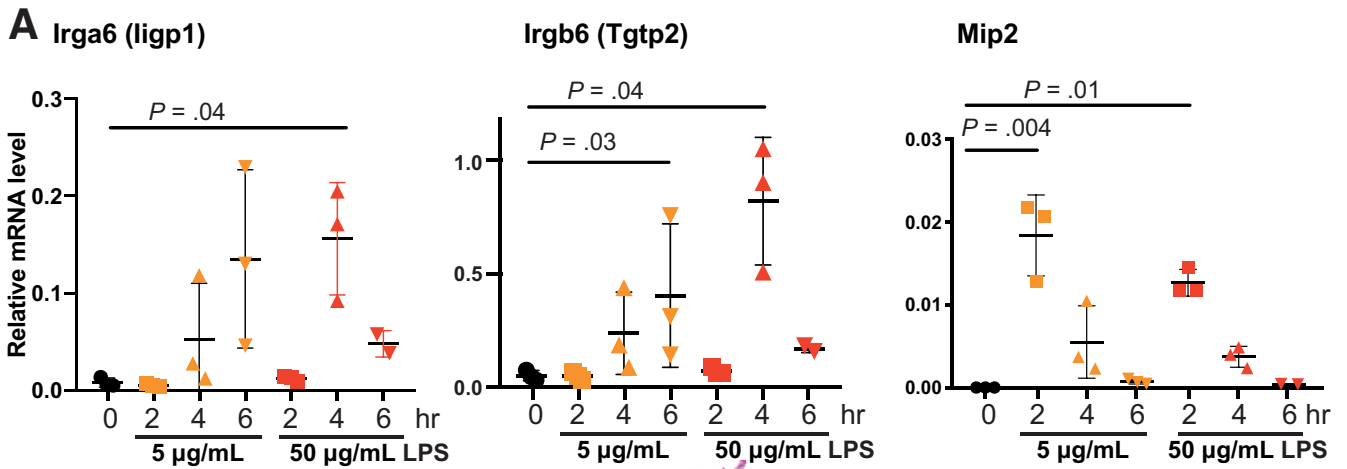
severe in the lower colon, this varies according to the molecular weight of DSS. A lower molecular weight (5 kilodaltons) of DSS is absorbed in the proximal colon/cecum and causes patchy lesions.[59] Therefore, the localization of sulindac-induced lesions in the mucosal folds of the proximal colon may be a combination of mechanical and biological factors.

Taken together, this study has provided evidence for the in vivo functional significance of MCC and has shown that the MCC knockout defect can drive carcinogenesis in the absence of β-catenin hyperactivity. It also has shown novel insights into the complexity of the inflammatory microenvironment that predisposes to malignancy in colorectal cancer.

Materials and Methods
Generation of New Mouse Lines

The Mcc-$loxP$ mouse line ($Mcc^{F/F}$) was generated by Ozgene (Bentley, WA, Australia) (Figure 1A) and designated B6.Cg-Mcc<tm1Maija>/Ausb. The 5' and 3' homology arms for the Mcc targeting vector were generated by PCR (Figure 1A). The first shared exon of the 2 main transcripts Mcc-201 (exon 4) and Mcc-202 (exon 2) was replaced by a partial complementary DNA (cDNA) modified from RIKEN clone E330037C1 (RIKEN, Saitama, Japan). This contained Mcc-201 exons 4–19, which correspond to Mcc-202 exons 2–17. The PGK-Neo selection, eGFP reporter, and STOP cassettes were inserted downstream of the cDNA. The targeting construct was electroporated into a C57BL/6 embryonic stem (ES) cell line, Bruce4.[60] Homologous recombinant ES cell clones were identified by Southern hybridization and injected into blastocysts. Male chimeric mice were obtained and crossed to C57BL/6J females to establish heterozygous germline offspring on a C57BL/6 background. The germline mice were crossed to a ubiquitous FLP C57BL/6 mouse line to remove the FRT flanked selectable marker cassette. MCC expressed by the $Mcc^{F/F}$ mice is driven from the endogenous Mcc-202 promoter but partially derived from the cDNA sequence. The long isoform Mcc-201 is not expressed in the colon of WT or $Mcc^{F/F}$ mice.

All subsequent breeding was performed at Australian BioResources (Moss Vale, Australia) in specific pathogenfree conditions, on a C57BL/6J strain background. $Mcc^{F/F}$ mice were crossed with the cre-deleter mice (B6.C-Tg [CMV-cre]1Cgn/J)[61] to generate the whole-body knockout line ($Mcc^{\Delta/\Delta}$). The loxP-flanked region is deleted in creexpressing mice and translation is terminated after the eGFP sequence. Two truncated fluorescent protein isoforms are expected but the transcripts appear to be unstable with no protein produced. Absence of the MCC protein was confirmed by Western blot in $Mcc^{\Delta/\Delta}$ mice. The major organs of four 40- to 47-week-old $Mcc^{\Delta/\Delta}$ mice were analyzed by the Australian Phenomics Network (IMVS Veterinary Pathology, Adelaide, Australia).

For the sulindac diet experiments, $Mcc^{F/F}$ were crossed with mice carrying the $Vilcre$ transgene (B6.SJL-Tg[vil-cre] 997Gum/J) (Jackson Laboratories, Bar Harbor, ME).[23] A 2-generation breeding protocol produced 4 genotypes: $VilcreMcc^{F/F}$ ($Mcc^{\Delta IEC}$), $VilcreMcc^{F/WT}$ ($Mcc^{\Delta IEC/WT}$), $Mcc^{F/F}$, and $Mcc^{F/WT}$. The animal experimentation was approved by the Garvan Institute Animal Ethics Committee.

For generation of MEF lines, $Mcc^{\Delta/WT}$ mice were crossed to obtain $Mcc^{\Delta/\Delta}$ and Mcc-WT embryos. MEFs were prepared from 13.5-day-old embryos and serially passaged in Dulbecco's modified Eagle media with 10% fetal bovine serum until they were immortalized.[62] Experiments were conducted with immortalized MEFs.

Genotyping protocol with primers Mcc-loxP-F1 (CCCAAACTCATGTGTGTTGTTCC) and Mcc-loxP-R1 (CCTTCCCTTTCTTCCTGTGATTAGC) produced a 182-bp fragment for the Mcc^{Δ}, a 162-bp fragment for Mcc^{F}, and a 103-bp fragment for Mcc-WT alleles.

In Vivo Proliferation Assay

$Mcc^{\Delta/\Delta}$ and wild-type siblings (Mcc-WT) were obtained from heterozygous crossings. Twenty-week-old mice were injected intraperitoneally with 100 mg/kg BrdU (Sigma-Aldrich, St. Louis, MO) and killed 2 hours after injection. The ileum and colon were harvested and fixed in 10% formalin for immunohistochemistry. Epitope retrieval was performed in a pressure cooker at 125°C with DAKO (Glostrup, Denmark) buffer S2367, pH 9.0 for 2 minutes. The primary antibody for BrdU (1:50, DAKO) was incubated for 60 minutes. The number of BrdU-positive cells in each crypt were counted and divided by the total number of cells in each crypt to obtain the percentage of BrdU positivity.

Figure 6. (*See previous page*). **Inflammation induces strong expression of *Irg* antimicrobial host defense genes in the colonic epithelium.** (A) Lipopolysaccharide (LPS) treatment in vitro up-regulates the expression of *Irga6*, *Irgb6*, and the chemokine *Mip2* in mouse CT26 cells. The cells were treated with 5–50 μg/mL LPS and harvested for RNA extraction and qPCR. mRNA levels were normalized to *Gapdh*. The graphs show a representative experiment with 3 replicates. Friedman's analysis of variance with a post hoc test for significant means was used to determine statistical significance. Error bars indicate the means with SD. (B–E) Immunohistochemical images of IRGA6 staining in the colon of a drug-treated $Mcc^{F/F}$ mouse. (B) Expression in the cytoplasm of isolated plasma cells and endothelium of blood vessels, but no expression in the normal colon. (C) Strong expression in the stromal and epithelial cells in an area of inflammation and erosion of the epithelial layer. (D) Strong expression in the stromal cells in an area of ulceration but weak focal expression in adenocarcinoma (*arrows*). (E) Strong expression of enterocytes in the colon epithelium (*white arrow*) next to inflammation. No IRGA6 expression in the epithelial cells away from inflammation (*purple arrow*) or in the neutrophils and lymphocytes (*black arrow*). (F and G) Immunohistochemical images of IRGM3 staining in the mouse colon ($Mcc^{F/F}$). (F) Expression in the cytoplasm of isolated plasma cells and endothelium of blood vessels but not in the healthy colonic epithelium. (G) Inflammation induced IRGM3 expression in the colonic epithelium. Expression also was seen in infiltrating plasma cells and macrophages. All images were taken with a Carl Zeiss Axio A2 Digital microscope with EC Plan-NEOFLUAR objectives and Carl Zeiss Axiocam HRc camera (Zeiss, Oberkochen, Germany). Original magnification, (E–G) ×400, (B–D) ×100.

Twenty crypts were counted for each individual mouse and colon region.

Mouse Experimentation and Colon Tissue Analysis

Sulindac (320 ppm; Sigma-Aldrich) was mixed with standard chow by Specialty Feeds (Glen Forrest, Western Australia). Six-week-old mice were given feed containing sulindac or standard chow and killed after 20 weeks of sulindac exposure. The number and size of visible lesions in the proximal colon were determined under a dissecting microscope. The colon lesions underwent a biopsy examination (2–13/mouse) together with control specimens (20–22 mice per group, both males and females).[16,18] After formalin fixation, processing, and sectioning using routine diagnostic laboratory methods, at least 2 H&E-stained sections per animal were analyzed by a specialist anatomical pathologist (J.E.D.) in a blinded fashion. For each biopsy specimen the features assessed included the following: type of inflammation (acute and/or chronic) and depth and severity of inflammation (absent, mild, moderate, or severe). Mucosal ulceration was regarded as severe acute inflammation and was defined as loss of the colonic mucosa associated with an acute inflammatory reaction extending at least through the muscularis mucosae. Mucosal erosion was regarded as moderate acute inflammation and was defined as superficial ulceration that involved only the surface epithelium and superficial underlying lamina propria. Epithelial dysplasia was graded as negative, indefinite for low-grade dysplasia, low-grade, or high-grade dysplasia according to the Riddell classification. Only biopsy specimens that showed neoplastic glands within a desmoplastic stroma extending beyond the muscularis mucosae were regarded as invasive cancer (invasive adenocarcinoma).[16,18]

For E-cadherin and β-catenin protein expression, heat-induced epitope retrieval of 3-μm tissue sections was performed for 25 seconds in a pressure cooker (total time, 30 min) using a citrate buffer at pH 6.0 (S1699; DAKO). The primary antibody was biotinylated with anti-mouse Fab fragment using the DAKO Animal Research Kit. The primary antibody for E-cadherin (1:500, 610181; BD Biosciences, Franklin Lakes, NJ) was incubated for 90 minutes, and for β-catenin (1:500, 610153; BD Biosciences) for 60 minutes. For AHR expression, heat retrieval of 3-μm tissue sections was performed for 48 minutes in CC1 buffer, with blocking for 8 minutes. Sections were stained with 1:50 dilution AHR antibody (ab84833; Abcam, Cambridge, UK). Ventana's OptiView 3,3′-diaminobenzidine tetra hydrochloride Immunohistochemistry Detection Kit was used to amplify and visualize the signals (Ventana, Roche, Basel, Switzerland). Omitting the primary antibody was the negative control and mouse prostate was the positive control. The slides were counterstained with hematoxylin.

For IRGA6 and IRGM3, heat-induced epitope retrieval of 3-μm tissue sections was performed for 10 minutes at 95ºC using Tris-EDTA buffer at pH 9.0. Detection of the primary antibodies, the anti-Irga6 serum (1:8000),[63] and anti-Irgm3 (1:100, sc-136317; Santa Cruz, Dallas, TX), was achieved with the ImmPRESS system (MP-7401; Vector, Burlingame,

CA). The horseradish-peroxidase color reaction was performed with the peroxidase substrate kit HistoGreen (E109; Linaris, WertheimBettingen, Germany). The nuclei were counterstained with Nuclear Fast Red.

Mouse Transcriptome and Pathway Analysis

A subset of mice (5–8 per group, all males) was killed after 10 weeks of sulindac exposure and the colon mucosa was harvested by light scraping and snap-frozen. RNA was extracted (74104, RNeasy mini kit; Qiagen, Hilden, Germany). Gene expression profiling was conducted using Mouse Transcriptome Array 1.0 (Affymetrix) at the Ramaciotti Centre for Genomics (Sydney, Australia). Quality control was performed using the Affymetrix Expression Console. Normalization and probe-set summarization was performed using the robust multichip average method of the Affymetrix Power Tools apt-probe set-summarize software (version 1.16.1) (using the -a rma option) resulting in 72,688 transcript clusters. Mouse gene symbols were assigned to each transcript cluster using Affymetrix NetAfx annotations (version na34.1 mm10). Differential expression between experimental groups was assessed using limma via the limmaGP tool in GenePattern (Broad Institute, San Diego, CA).[64] Mouse gene symbols were mapped to human orthologs using version 78 of the Ensembl database (EMBL-EBI, Hinxton, UK). The transcript profiling data have been deposited at NCBI Gene Expression Omnibus (GSE84391–GEO) and is freely available at http://www.ncbi.nlm.nih.gov/geo/query/acc.cgi?token=kzwlcwasldsrfen&acc=GSE84391.

Functionally associated gene sets were identified using GSEA on a ranked list of the limma moderated t statistics, from each pair-wise comparison, against the 50 Hallmark gene sets from v5.0 of the MSigDB (Broad Institute).[26] The most significantly down-regulated genes ($Q < 0.05$) in recognized DNA repair pathways were further identified with network analyses of the $Mcc^{\Delta IEC}$ data (STRING, Cytoscape, KEGG) and pathway annotations in GeneCards.

Comparison of Sulindac-Induced Colon Inflammation and the DSS Colitis Model

Publicly available raw gene expression data from a previous DSS colitis experiment[34] were downloaded from GEO (accession GSE22307). Robust Multi-array Average (RMA) values were generated and differential expression between days 0 and 6 of DSS treatment was determined using limma[65] and compared with the data from this study ($Mcc^{F/F}$). A probe set was considered differentially expressed in either study if $Q < 0.05$. The official gene symbol was used to map between array platforms, providing a total of 18,898 probe sets. Log fold-change between the end points and controls were plotted for probe sets that were differentially expressed in 1 or both of the studies. Correlations were calculated using the Pearson correlation coefficient (r).

qPCR Analysis

cDNA was prepared using the Quantitect Reverse Transcription Kit (205311; Qiagen). Gene expression changes in

the mouse colon mucosa were validated with qPCR[16–18] from 3–6 mice/group. In vitro validation of *Irg* gene expression was conducted using mouse colon cancer cells CT26.WT (CRL-2638; ATCC, Manassas, VA), which were treated with 5–50 μg/mL lipopolysaccharide (InvivoGen, San Diego, CA) for 2–6 hours. Expression of DNA damage response genes was analyzed in MEFs, treated with 400 μmol/L H_2O_2 (AJA260; ThermoFisher, Waltham, MA) for 1–6 hours. The qPCR was always conducted in triplicate for each specimen.

The following TaqMan assays (Life Technologies, Carlsbad, CA) were used: Mm01262684_m1 (*Mcc*), Mm01168399_m1 (*Mmp10*), Mm00439491_m1 (*Mmp13*), Mm00443610_m1 (*Axin2*), Mm00438889_m1 (*Lgr5*), and Mm99999915_g1 (*Gapdh*).

Universal Probe Library (UPL; Roche Applied Science, Mannheim, Germany) assay primers and probes were as follows: *Tgtp2*_forward (F) (ccagatcaaggtcaccactg), *Tgtp2*_reverse (R) (gagatgattttgctttccctttt), UPL probe 78; *Iigp1*_3_F (tgtttggagtggatgaaacatct), *Iigp1*_3_R (cctccacctgatccacctc), UPL probe 48; *Atm*_F (tgcagatttatatccatcatccac), *Atm*_R (tttcatggattcataagcacctt), UPL probe 106; *Rad1*_F (tgtctcctgacaagccctattt), *Rad1*_R (tgttgacctgggtcttatcaca), UPL probe 31; *Mlh1*_F (gttttactccattcggaagca), *Mlh1*_R (ggagccaggcatgtcact), UPL probe 25; *Msh2*_F (gctgggatgtgacgaagc), *Msh2*_R (cagaataattttctcaccttgctct), UPL probe 27; *Msh3*_F (ttgaaataaagaactcggctgtatc), *Msh3*_R (ggctcacagcttttgtgtct), UPL probe 33; *Cyp2c68*_F (acattggccagtgccttact), *Cyp2c68*_R (ggcttctttcattgcctcat), UPL probe 100; and *Mip2* left (aaaatcatccaaaagatactgaacaa), *Mip2* right (ctttggttcttccgttgagg), UPL probe 26.

Cell Cycle and Protein Analysis

MCC was stably knocked down in HCT116 (CCL-247; ATCC) colon cancer cells using the Mission short hairpin RNA Human Gene Family Set (SHCLNG-NM_002387; Sigma-Aldrich) and a lentiviral transduction method (MCC-KD cells).[11,66] MCC-KD and NT cells were dosed with 10 J/m^2 UV radiation (UV-C) using a UV Stratalinker 1800 (Stratagene, La Jolla, CA). MEFs were treated with 400 or 600 μmol/L H_2O_2 for up to 6 hours or treated with 400 μmol/L for 2 hours and then allowed to recover in fresh medium. Cell-cycle distribution was measured by flow cytometric analysis of propidium iodide–stained, ethanol-fixed cells on a BD FACS Canto II (BD Biosciences) using Cell Quest (BD Biosciences) and ModFit (Verity Software, Topsham, ME). Western blots were probed with antibodies raised to MCC (610740, BD Biosciences), pChk2-T68, pChk1-Ser345, pRb807/811 (2661, 2341, 8516; Cell Signaling, Danvers, MA), Rb (554136; BD Pharmingen, BD Biosciences), and γH2AX (10856-1-AP; Proteintech, Rosemont, IL).

Comet Assay

The comet assay was performed using the CometAssay Reagent Kit for Single Cell Gel Electrophoresis Assay following the manufacturer's instructions (4250-050-01; Trevigen, Gaithersburg, MD). Exponentially growing cells were treated with 10 nmol/L to 1 μmol/L SN38 (Selleck Chemicals, Houston, TX) for 2 hours. High-resolution images of the comets formed were generated using the Leica DM 6000 Power Mosaic microscope (Leica Microsystems, Wetzlar, Germany). Tail length was quantified using the Open-Comet v1.3 ImageJ (National Institutes of Health, Bethesda, MD) plug-in from comets generated from 3 independent experiments.

Statistical Analysis

Differences in messenger RNA/protein expression, epithelial proliferation, number/size of lesions, cell-cycle phases, and comet tail lengths were compared using *t* tests, analysis of variance or the corresponding nonparametric tests, and all frequencies with the Fisher exact test (GraphPad Prism, San Diego, CA). $P < .05$ was considered significant. In bioinformatics analyses the significance was corrected for multiple comparisons and $Q < 0.05$ was considered significant.

All authors had access to the study data and reviewed and approved the final manuscript.

References

1. Terzic J, Grivennikov S, Karin E, Karin M. Inflammation and colon cancer. Gastroenterology 2010; 138:2101–2114 e5.
2. Kinzler KW, Nilbert MC, Vogelstein B, Bryan TM, Levy DB, Smith KJ, Preisinger AC, Hamilton SR, Hedge P, Markham A, et al. Identification of a gene located at chromosome 5q21 that is mutated in colorectal cancers. Science 1991;251:1366–1370.
3. Fukuyama R, Niculaita R, Ng KP, Obusez E, Sanchez J, Kalady M, Aung PP, Casey G, Sizemore N. Mutated in colorectal cancer, a putative tumor suppressor for serrated colorectal cancer, selectively represses beta-catenin-dependent transcription. Oncogene 2008;27:6044–6055.
4. Kohonen-Corish MR, Sigglekow ND, Susanto J, Chapuis PH, Bokey EL, Dent OF, Chan C, Lin BP, Seng TJ, Laird PW, Young J, Leggett BA, Jass JR, Sutherland RL. Promoter methylation of the mutated in colorectal cancer gene is a frequent early event in colorectal cancer. Oncogene 2007;26:4435–4441.
5. Lim L, Balakrishnan A, Huskey N, Jones KD, Jodari M, Ng R, Song G, Riordan J, Anderton B, Cheung ST, Willenbring H, Dupuy A, Chen X, Brown D, Chang AN, Goga A. MicroRNA-494 within an oncogenic microRNA megacluster regulates G1/S transition in liver tumorigenesis through suppression of mutated in colorectal cancer. Hepatology 2014;59:202–215.
6. Shukla R, Upton KR, Munoz-Lopez M, Gerhardt DJ, Fisher ME, Nguyen T, Brennan PM, Baillie JK, Collino A, Ghisletti S, Sinha S, Iannelli F, Radaelli E, Dos Santos A, Rapoud D, Guettier C, Samuel D, Natoli G, Carninci P, Ciccarelli FD, Garcia-Perez JL, Faivre J, Faulkner GJ. Endogenous retrotransposition activates oncogenic pathways in hepatocellular carcinoma. Cell 2013;153:101–111.
7. Pangon L, Mladenova D, Watkins L, Van Kralingen C, Currey N, Al-Sohaily S, Lecine P, Borg JP, Kohonen-Corish MR. MCC inhibits beta-catenin transcriptional activity by sequestering DBC1 in the cytoplasm. Int J Cancer 2015;136:55–64.

8. Pangon L, Sigglekow ND, Larance M, Al-Sohaily S, Mladenova DN, Selinger CI, Musgrove EA, Kohonen-Corish MR. The "mutated in colorectal cancer" protein is a novel target of the UV-induced DNA damage checkpoint. Genes Cancer 2010;1:917–926.

9. Pangon L, Van Kralingen C, Abas M, Daly RJ, Musgrove EA, Kohonen-Corish MR. The PDZ-binding motif of MCC is phosphorylated at position-1 and controls lamellipodia formation in colon epithelial cells. Biochim Biophys Acta 2012;1823:1058–1067.

10. Sigglekow ND, Pangon L, Brummer T, Molloy M, Hawkins NJ, Ward RL, Musgrove EA, Kohonen-Corish MR. Mutated in colorectal cancer protein modulates the NFkappaB pathway. Anticancer Res 2012;32:73–79.

11. Benthani FA, Herrmann D, Tran PN, Pangon L, Lucas MC, Allam AH, Currey N, Al-Sohaily S, Giry-Laterriere M, Warusavitarne J, Timpson P, Kohonen-Corish MRJ. 'MCC' protein interacts with E-cadherin and beta-catenin strengthening cell-cell adhesion of HCT116 colon cancer cells. Oncogene 2018; 37:663–672.

12. Li L, Fu X, Zhang W, Xiao L, Qiu Y, Peng Y, Shi L, Chen X, Zhou X, Deng M. Wnt signaling pathway is activated in right colon serrated polyps correlating to specific molecular form of beta-catenin. Hum Pathol 2013; 44:1079–1088.

13. Murakami T, Mitomi H, Saito T, Takahashi M, Sakamoto N, Fukui N, Yao T, Watanabe S. Distinct WNT/beta-catenin signaling activation in the serrated neoplasia pathway and the adenoma-carcinoma sequence of the colorectum. Mod Pathol 2015;28:146–158.

14. Bard-Chapeau EA, Nguyen AT, Rust AG, Sayadi A, Lee P, Chua BQ, New LS, de Jong J, Ward JM, Chin CK, Chew V, Toh HC, Abastado JP, Benoukraf T, Soong R, Bard FA, Dupuy AJ, Johnson RL, Radda GK, Chan EC, Wessels LF, Adams DJ, Jenkins NA, Copeland NG. Transposon mutagenesis identifies genes driving hepatocellular carcinoma in a chronic hepatitis B mouse model. Nat Genet 2014;46:24–32.

15. Starr TK, Allaei R, Silverstein KA, Staggs RA, Sarver AL, Bergemann TL, Gupta M, O'Sullivan MG, Matise I, Dupuy AJ, Collier LS, Powers S, Oberg AL, Asmann YW, Thibodeau SN, Tessarollo L, Copeland NG, Jenkins NA, Cormier RT, Largaespada DA. A transposon-based genetic screen in mice identifies genes altered in colorectal cancer. Science 2009;323:1747–1750.

16. Mladenova D, Daniel JJ, Dahlstrom JE, Bean E, Gupta R, Pickford R, Currey N, Musgrove EA, Kohonen-Corish MR. The NSAID sulindac is chemopreventive in the mouse distal colon but carcinogenic in the proximal colon. Gut 2011;60:350–360.

17. Mladenova D, Pangon L, Currey N, Ng I, Musgrove EA, Grey ST, Kohonen-Corish MR. Sulindac activates NF-kappaB signaling in colon cancer cells. Cell Commun Signal 2013;11:73.

18. Mladenova DN, Dahlstrom JE, Tran PN, Benthani F, Bean EG, Ng I, Pangon L, Currey N, Kohonen-Corish MR. HIF1alpha deficiency reduces inflammation in a mouse model of proximal colon cancer. Dis Model Mech 2015;8:1093–1103.

19. Greenspan EJ, Nichols FC, Rosenberg DW. Molecular alterations associated with sulindac-resistant colon tumors in ApcMin/+ mice. Cancer Prev Res (Phila) 2010; 3:1187–1197.

20. Rice PL, Kelloff J, Sullivan H, Driggers LJ, Beard KS, Kuwada S, Piazza G, Ahnen DJ. Sulindac metabolites induce caspase- and proteasome-dependent degradation of beta-catenin protein in human colon cancer cells. Mol Cancer Ther 2003;2:885–892.

21. Yang K, Fan K, Kurihara N, Shinozaki H, Rigas B, Augenlicht L, Kopelovich L, Edelmann W, Kucherlapati R, Lipkin M. Regional response leading to tumorigenesis after sulindac in small and large intestine of mice with Apc mutations. Carcinogenesis 2003;24:605–611.

22. Itano O, Yang K, Fan K, Kurihara N, Shinozaki H, Abe S, Jin B, Gravaghi C, Edelmann W, Augenlicht L, Kopelovich L, Kucherlapati R, Lamprecht S, Lipkin M. Sulindac effects on inflammation and tumorigenesis in the intestine of mice with Apc and Mlh1 mutations. Carcinogenesis 2009;30:1923–1926.

23. Madison BB, Dunbar L, Qiao XT, Braunstein K, Braunstein E, Gumucio DL. Cis elements of the villin gene control expression in restricted domains of the vertical (crypt) and horizontal (duodenum, cecum) axes of the intestine. J Biol Chem 2002;277:33275–33283.

24. Gabrilovich DI, Ostrand-Rosenberg S, Bronte V. Coordinated regulation of myeloid cells by tumours. Nat Rev Immunol 2012;12:253–268.

25. Lamouille S, Xu J, Derynck R. Molecular mechanisms of epithelial-mesenchymal transition. Nat Rev Mol Cell Biol 2014;15:178–196.

26. Liberzon A, Birger C, Thorvaldsdottir H, Ghandi M, Mesirov JP, Tamayo P. The Molecular Signatures Database (MSigDB) hallmark gene set collection. Cell Syst 2015;1:417–425.

27. Guinney J, Dienstmann R, Wang X, de Reynies A, Schlicker A, Soneson C, Marisa L, Roepman P, Nyamundanda G, Angelino P, Bot BM, Morris JS, Simon IM, Gerster S, Fessler E, De Sousa EMF, Missiaglia E, Ramay H, Barras D, Homicsko K, Maru D, Manyam GC, Broom B, Boige V, Perez-Villamil B, Laderas T, Salazar R, Gray JW, Hanahan D, Tabernero J, Bernards R, Friend SH, Laurent-Puig P, Medema JP, Sadanandam A, Wessels L, Delorenzi M, Kopetz S, Vermeulen L, Tejpar S. The consensus molecular subtypes of colorectal cancer. Nat Med 2015;21:1350–1356.

28. Barker N, van de Wetering M, Clevers H. The intestinal stem cell. Genes Dev 2008;22:1856–1864.

29. Walker F, Zhang HH, Odorizzi A, Burgess AW. LGR5 is a negative regulator of tumourigenicity, antagonizes Wnt signalling and regulates cell adhesion in colorectal cancer cell lines. PLoS One 2011;6:e22733.

30. Davidson LA, Goldsby JS, Callaway ES, Shah MS, Barker N, Chapkin RS. Alteration of colonic stem cell gene signatures during the regenerative response to injury. Biochim Biophys Acta 2012;1822:1600–1607.

31. Bacher JW, Abdel Megid WM, Kent-First MG, Halberg RB. Use of mononucleotide repeat markers for detection of microsatellite instability in mouse tumors. Mol Carcinog 2005;44:285–292.

32. Currey N, Daniel JJ, Mladenova DN, Dahlstrom JE, Kohonen-Corish MRJ. Microsatellite instability in mouse models of colorectal cancer. Can J Gastroenterol Hepatol 2018;2018:6152928.

33. Schwarz JK, Lovly CM, Piwnica-Worms H. Regulation of the Chk2 protein kinase by oligomerization-mediated cis- and trans-phosphorylation. Mol Cancer Res 2003; 1:598–609.

34. Fang K, Bruce M, Pattillo CB, Zhang S, Stone R 2nd, Clifford J, Kevil CG. Temporal genomewide expression profiling of DSS colitis reveals novel inflammatory and angiogenesis genes similar to ulcerative colitis. Physiol Genomics 2011;43:43–56.

35. Saleh M, Trinchieri G. Innate immune mechanisms of colitis and colitis-associated colorectal cancer. Nat Rev Immunol 2011;11:9–20.

36. Lilue J, Muller UB, Steinfeldt T, Howard JC. Reciprocal virulence and resistance polymorphism in the relationship between Toxoplasma gondii and the house mouse. Elife 2013;2:e01298.

37. McCarroll SA, Huett A, Kuballa P, Chilewski SD, Landry A, Goyette P, Zody MC, Hall JL, Brant SR, Cho JH, Duerr RH, Silverberg MS, Taylor KD, Rioux JD, Altshuler D, Daly MJ, Xavier RJ. Deletion polymorphism upstream of IRGM associated with altered IRGM expression and Crohn's disease. Nat Genet 2008; 40:1107–1112.

38. Kohonen-Corish MR, Daniel JJ, te Riele H, Buffinton GD, Dahlstrom JE. Susceptibility of Msh2-deficient mice to inflammation-associated colorectal tumors. Cancer Res 2002;62:2092–2097.

39. Young T, Poobalan Y, Ali Y, Siew Tein W, Sadasivam A, Ee Kim T, Erica Tay P, Dunn NR. Mutated in colorectal cancer (Mcc), a candidate tumor suppressor, is dynamically expressed during mouse embryogenesis. Dev Dyn 2011;240:2166–2174.

40. Gaillard H, Garcia-Muse T, Aguilera A. Replication stress and cancer. Nat Rev Cancer 2015;15:276–289.

41. Chang CL, Marra G, Chauhan DP, Ha HT, Chang DK, Ricciardiello L, Randolph A, Carethers JM, Boland CR. Oxidative stress inactivates the human DNA mismatch repair system. Am J Physiol Cell Physiol 2002; 283:C148–C154.

42. Hawn MT, Umar A, Carethers JM, Marra G, Kunkel TA, Boland CR, Koi M. Evidence for a connection between the mismatch repair system and the G2 cell cycle checkpoint. Cancer Res 1995;55:3721–3725.

43. Bracken AP, Ciro M, Cocito A, Helin K. E2F target genes: unraveling the biology. Trends Biochem Sci 2004; 29:409–417.

44. Bertoli C, Herlihy AE, Pennycook BR, Kriston-Vizi J, de Bruin RAM. Sustained E2F-dependent transcription is a key mechanism to prevent replication-stress-induced DNA damage. Cell Rep 2016;15:1412–1422.

45. Bertoli C, Klier S, McGowan C, Wittenberg C, de Bruin RA. Chk1 inhibits E2F6 repressor function in response to replication stress to maintain cell-cycle transcription. Curr Biol 2013;23:1629–1637.

46. Herlihy AE, de Bruin RA. The role of the transcriptional response to DNA replication stress. Genes (Basel) 2017;8.

47. Ren B, Cam H, Takahashi Y, Volkert T, Terragni J, Young RA, Dynlacht BD. E2F integrates cell cycle progression with DNA repair, replication, and G(2)/M checkpoints. Genes Dev 2002;16:245–256.

48. Coers J, Bernstein-Hanley I, Grotsky D, Parvanova I, Howard JC, Taylor GA, Dietrich WF, Starnbach MN. Chlamydia muridarum evades growth restriction by the IFN-gamma-inducible host resistance factor Irgb10. J Immunol 2008;180:6237–6245.

49. Ferreira-da-Silva Mda F, Springer-Frauenhoff HM, Bohne W, Howard JC. Identification of the microsporidian Encephalitozoon cuniculi as a new target of the IFNgamma-inducible IRG resistance system. PLoS Pathog 2014;10:e1004449.

50. Man SM, Karki R, Sasai M, Place DE, Kesavardhana S, Temirov J, Frase S, Zhu Q, Malireddi RK, Kuriakose T, Peters JL, Neale G, Brown SA, Yamamoto M, Kanneganti TD. IRGB10 liberates bacterial ligands for sensing by the AIM2 and caspase-11-NLRP3 inflammasomes. Cell 2016;167:382–396 e17.

51. Taylor GA, Feng CG, Sher A. p47 GTPases: regulators of immunity to intracellular pathogens. Nat Rev Immunol 2004;4:100–109.

52. Brest P, Lapaquette P, Souidi M, Lebrigand K, Cesaro A, Vouret-Craviari V, Mari B, Barbry P, Mosnier JF, Hebuterne X, Harel-Bellan A, Mograbi B, Darfeuille-Michaud A, Hofman P. A synonymous variant in IRGM alters a binding site for miR-196 and causes deregulation of IRGM-dependent xenophagy in Crohn's disease. Nat Genet 2011;43:242–245.

53. Georges M. The long and winding road from correlation to causation. Nat Genet 2011;43:180–181.

54. Perse M, Cerar A. Dextran sodium sulphate colitis mouse model: traps and tricks. J Biomed Biotechnol 2012; 2012:718617.

55. Safe S, Lee SO, Jin UH. Role of the aryl hydrocarbon receptor in carcinogenesis and potential as a drug target. Toxicol Sci 2013;135:1–16.

56. Thiefin G, Beaugerie L. Toxic effects of nonsteroidal antiinflammatory drugs on the small bowel, colon, and rectum. Joint Bone Spine 2005;72:286–294.

57. Pilotto A, Seripa D, Franceschi M, Scarcelli C, Colaizzo D, Grandone E, Niro V, Andriulli A, Leandro G, Di Mario F, Dallapiccola B. Genetic susceptibility to nonsteroidal anti-inflammatory drug-related gastroduodenal bleeding: role of cytochrome P450 2C9 polymorphisms. Gastroenterology 2007;133: 465–471.

58. Lee SM, Kim N, Son HJ, Park JH, Nam RH, Ham MH, Choi D, Sohn SH, Shin E, Hwang YJ, Sung J, Lee DH, Lee HN. The effect of sex on the azoxymethane/dextran sulfate sodium-treated mice model of colon cancer. J Cancer Prev 2016;21:271–278.

59. Kitajima S, Takuma S, Morimoto M. Histological analysis of murine colitis induced by dextran sulfate sodium of different molecular weights. Exp Anim 2000;49:9–15.

60. Kontgen F, Suss G, Stewart C, Steinmetz M, Bluethmann H. Targeted disruption of the MHC class II Aa gene in C57BL/6 mice. Int Immunol 1993; 5:957–964.

61. Schwenk F, Baron U, Rajewsky K. A cre-transgenic mouse strain for the ubiquitous deletion of loxP-flanked gene segments including deletion in germ cells. Nucleic Acids Res 1995;23:5080–5081.

62. Sharpless NE. Preparation and immortalization of primary murine cells. In: Celis JE, ed. Cell biology: a laboratory handbook, vol 1. London: Elsevier Academic Press, 2006:223–228.

63. Papic N, Hunn JP, Pawlowski N, Zerrahn J, Howard JC. Inactive and active states of the interferon-inducible resistance GTPase, Irga6, in vivo. J Biol Chem 2008; 283:32143–32151.

64. Smyth GK. Linear models and empirical Bayes methods for assessing differential expression in microarray experiments. Stat Appl Genet Mol Biol 2004;3, article 3.

65. Ritchie ME, Phipson B, Wu D, Hu Y, Law CW, Shi W, Smyth GK. Limma powers differential expression analyses for RNA-sequencing and microarray studies. Nucleic Acids Res 2015;43:e47.

66. Pangon L, Ng I, Giry-Laterriere M, Currey N, Morgan A, Benthani F, Tran PN, Al-Sohaily S, Segelov E, Parker BL, Cowley MJ, Wright DC, St Heaps L, Carey L, Rooman I, Kohonen-Corish MR. JRK is a positive regulator of beta-catenin transcriptional activity commonly overexpressed in colon, breast and ovarian cancer. Oncogene 2016; 35:2834–2841.

Author contributions
Maija Kohonen-Corish was responsible for the study concept and design and obtained funding; Nicola Currey, Zeenat Jahan, C. Elizabeth Caldon, Phuong Tran, Fahad Benthani, Penelope De Lacavalerie, Daniel Roden, Brian Gloss, Claudia Campos, Elaine Bean, Amanda Bullman, Saskia Reibe-Pal, and Jane Dahlstrom acquired, analyzed, and interpreted data and performed the statistical analysis; Maija Kohonen-Corish, Jane Dahlstrom, and C. Elizabeth Caldon drafted the manuscript and critically revised the manuscript for important intellectual content; and Marcel Dinger, Mark Febbraio, and Stephen Clarke provided material support or resources.